Palaeoceanographic reconstruction of surface-ocean changes in the southern Norwegian Sea for the last ~130,000 years based on diatoms and with comparison to foraminiferal records

Ulrike Hoff[a,†], Tine L. Rasmussen[a,*], Hanno Meyer[b], Nalân Koç[c], Jesper Hansen[d]

[a] CAGE – Centre for Arctic Gas Hydrate, Environment and Climate, Department of Geosciences, UiT, The Arctic University of Norway, NO-9037 Tromsø, Norway
[b] Alfred Wegener Institute for Polar and Marine Research, Research Potsdam, Telegrafenberg A45-2, D-14473 Potsdam, Germany
[c] Norwegian Polar Institute, Fram Centre, Hjalmar Johansens gt. 14, NO-9296 Tromsø, Norway
[d] Akvaplan-niva AS, Fram Centre, Hjalmar Johansens gt. 14, NO-9296 Tromsø, Norway

ABSTRACT

Fossil marine diatom assemblages in a sediment core from the central northern Faroe slope in the Norwegian Sea were used to reconstruct palaeoceanographic changes in the surface water mixed layer from the last ~130,000 years (Marine Isotope Stage (MIS) 6/5 transition to MIS 1 (including the Eemian and Holocene interglacials) and to compare the results with previously published results on planktic foraminifera representing the subsurface conditions of the thermocline. Diatom floras from MIS 5 of the Nordic seas have rarely been studied in detail before and never the entire period from pre-Eemian to present. The composition of diatom species together with maxima in absolute abundance of diatoms, indicate two periods of warmer sea surface temperatures correlating with the Eemian and Holocene interglacials, respectively. The Eemian differs from the Holocene in that the Iceland-Faroe Front never developed, suggesting the cold East Icelandic Current (originating from the East Greenland Current) running north of Iceland was reduced or more mixed with Atlantic water than during the Holocene and that the surface temperature and salinity gradients were weaker. The northern Faroe slope was in the early Weichselian of MIS 5d–5a mainly influenced by weaker inflow of Atlantic water and stronger influence of the East Icelandic Current and by seasonal sea-ice cover. During the later part of the Weichselian (MIS 4–MIS 2) cold conditions prevailed with extensive sea-ice cover except during the warmer interstadials. The diatom floras were more sensitive to climate changes than the planktic foraminifera and indicate longer periods with warm surface conditions, and increased influence of the warm Atlantic surface water from the Faroe Current in MIS 5, suggesting a shallower and much steeper thermocline during the transitional periods compared to today. The diatoms are good indicators for Atlantic water inflow and possible convection in the Nordic seas, not merely reflecting orbital variations in insolation as previously suggested.

1. Introduction

Marine diatoms of the North Atlantic Ocean are very sensitive to changes in e.g., sea surface temperatures and sea-ice cover (e.g., Schrader et al., 1993a; Kohly, 1998; Jiang et al., 2001; Justwan and Koç, 2008; Krawczyk et al., 2017; Oksman et al., 2019), and salinity (Juggins, 1992), and have been used in numerous studies dealing with reconstructions of past palaeoceanographic changes. However, most studies from high-latitude marine sediments have focused on younger sediments from the late glacial and Holocene (e.g., Koç Karpuz and Schrader, 1990; Koç Karpuz and Jansen, 1992; Koç et al., 1993;

Schrader et al., 1993b; Jiang, 1996; Birks and Koç, 2002; Jiang et al., 2002; Andersen et al., 2004; Witak et al., 2005; Witon et al., 2006; Berner et al., 2008, 2011; Ran et al., 2008; Sha et al., 2011; Pearce et al., 2014; Krawczyk et al., 2017; Oksman et al., 2017) and in recent years mostly on the late Holocene (e.g., Krawczyk et al., 2010; Miettinen and Divine, 2012, Miettinen et al., 2015; Jiang et al., 2015; Orme et al., 2018). Temperature reconstructions based on different groups of microfossils such as planktic foraminifera, alkenones and coccospheres, radiolaria and diatoms give different results (Birks and Koç, 2002; Calvo et al., 2002; Dolven et al., 2002; Andrews and Giraudeau, 2003; Risebrobakken et al., 2003; Andersson et al., 2010).

This has been attributed to differences in living depth in the water column and differences in seasonality (see e.g., Moros et al., 2004; Andersson et al., 2010). In general at high latitudes, planktic foraminifera live deeper in the water column (e.g., *Neogloboquadrina pachyderma*, c. 50–200 m; e.g., Bé and Tolderlund, 1971; Hemleben et al., 1989; Bauch et al., 1997) than diatoms (< 50 m; Birks and Koç, 2002 and references therein) (e.g., Risebrobakken et al., 2011; Matul et al., 2018). This has led to the inference that a combination of these proxy signals is able to record changes in the Atlantic water at both the surface mixed layer and the subsurface thermocline, respectively.

The present investigation uses diatoms in comparison with planktic foraminifera to provide an overview about palaeoceanographic changes in the upper water column within the highly variable environment of the southern Norwegian Sea. We focus on the last ~130,000 years covering the MIS 6/5 transition to MIS 1 including the Eemian and Holocene interglacials and the Weichselian glacial comprising events of warm interstadials, cold stadials and glacial maxima (e.g., Shackleton and Opdyke, 1973; Dansgaard et al., 1993; Jouzel et al., 2003). Our study compares the results from the analyses of diatoms to previously published results of the distribution patterns of planktic foraminiferal species from nearby and near-identical core record ENAM93–21/MD95–2009 (Rasmussen et al., 1996a,b,c, 1999, 2003a,b). Core JM11-FI-19PC has previously been studied for stable isotope records of the planktic foraminifera, but no planktic faunal distribution data exist for this record (Ezat et al., 2014, 2016). Earlier studies of planktic foraminiferal census data from the Nordic seas (e.g., Kellogg et al., 1978; Belanger, 1982; Haake and Pflaumann, 1989; Fronval et al., 1998; Rasmussen et al., 1999) have shown that only in the Eemian and Holocene interglacials did the foraminifera record strong warming, while for the entire Weichselian period they indicated cold surface conditions with temperatures remaining below ~5 °C, also during the climatically warm interstadials. The purposes of the present diatom study is to 1) find evidence of surface water warming and Atlantic water inflow during MIS 5d–5a and MIS 4–2 and 2) obtain more details about changes in water mass structure of the upper water column during MIS 5–1 by comparison of surface dwelling diatom floras with the deeper-dwelling planktic foraminifera. The overall purpose is to gain a better understanding of palaeoenvironmental and -climatic changes in the Nordic seas over the last ~130,000 years.

2. Oceanographic setting

The deep-water formation in the Nordic seas constitutes an important part of the North Atlantic thermohaline circulation (e.g., Broecker and Denton, 1989; Broecker, 1991; Alonso-Garcia et al., 2011). The North Atlantic Current (NAC), the upper limb of the ocean circulation system, transports warm, saline Atlantic surface Water northwards across the Greenland-Scotland Ridge into the Nordic seas, while cold, low-salinity Polar surface Water flows out south along East Greenland as the East Greenland Current (EGC) (Fig. 1). The Atlantic surface Water cools and sinks to form deep and intermediate water masses. The cold, dense waters overflow the Greenland-Scotland Ridge, contributing to North Atlantic Deep Waters.

Polar surface Water is characterized by temperatures < 2 °C and salinity 33.0–34.4‰ (Hopkins, 1991). In the central part of the Nordic seas, the Polar and the warm and saline Atlantic surface Water are mixed, creating the Arctic surface Water characterized by temperatures < 8 °C and salinity 34.6–34.9‰ (Hopkins, 1991). These three surface water masses are separated by oceanic fronts, where lateral and vertical mixing occurs (Hansen and Østerhus, 2000). The northernmost front, the Polar Front, is located where the Polar and the Arctic surface Water masses meet. The Arctic Front is located where the Arctic surface Water and the Atlantic surface Water masses meet (e.g., Jansen and Bjørklund, 1985; Swift, 1986; Hopkins, 1991; Fronval and Jansen, 1996; Hebbeln et al., 1998; Hansen and Østerhus, 2000; Ślubowska-Woldengen et al., 2007; Mukhina and Dmitrenko, 2008) (Fig. 1). The

Atlantic water is ice-free throughout the year, while the Arctic water has seasonal, and the Polar water permanent or near-permanent sea-ice cover (Hansen and Østerhus, 2000; Deser and Teng, 2008). Seasonal phytoplankton productivity is very low in the Polar water, while intermediate to high productivity is found in the Atlantic water south of the Arctic Front. The highest productivity occurs at the Arctic Front and the less ice covered part of the Arctic water (Smith et al., 1985; Reigstad et al., 2011).

3. Study area

The Faroe Islands are located west of the Faroe-Shetland Channel (61°24′–62°24′N and 6°15′–7°41′W) (Fig. 1). The archipelago is presently affected by a strongly maritime climate with warm winters and cool summers. The average air temperature is 3.2 °C for January and 10.5 °C for August with dominating south-westerly winds (Søgaard, 1996). The eastern part of the Faroe-Shetland Channel is characterized by saline (> 35‰ Dooley and Meincke, 1981; Van Aken, 1988) and warm surface water with a typical temperature range of 6 to 10.5 °C, derived from the North Atlantic Water (NAW) (Hansen et al., 1998; Hansen and Østerhus, 2000) (Fig. 1). The water mass over the western and northern Faroe shelf and slope is normally dominated by the Faroe Current with inflowing warm Atlantic Water with a temperature of 7–8.5 °C (Fig. 1). The Iceland-Faroe Front, constitutes the border between the Faroe Current, and the fresher and colder mixture of Arctic surface Water coming by the East Icelandic Current (EIC) from the EGC and recirculated Atlantic Water from the Irminger Current and the Faroe Current itself (Hansen and Østerhus, 2000) (Fig. 1).

The Faroe Current has its origin within the NAC with temperature 9.5–10.5 °C and salinity 35.35–35.45‰ (Hansen and Østerhus, 2000) (Fig. 1). The strength of the NAC is generally related to the deep-water formation in the Nordic seas and the strength of the cold overflows (Hansen and Østerhus, 2000). The flow of the NAC is weaker and may get displaced during periods of freshening of the surface waters caused by a strong input of Polar Water from the EGC as well as the EIC (e.g., Malmberg, 1985; Andersen et al., 2004).

A CTD (Conductivity, Temperature, Depth)-cast from April 30, 2011 from the northern Faroe margin shows a typical record for the area (e.g., Hansen and Østerhus, 2000) with an upper wind-generated mixed layer at 0–50 m water depth with a temperature of ~8 °C and salinity of 35.25‰ indicative of modified North Atlantic surface Water (Fig. 2). Due to unusually calm spring conditions of April–May 2011, a thin layer (~10 m) of warm (8.6 °C) and less salty water (35.24‰) is found on top of the mixed layer. The Atlantic Water layer reaches to 500 m water depth overlaying the cold, dense overflow water (temperature −0.5 °C, salinity 34.9‰, density 28.5 kg/m^3) (Fig. 2).

4. Material and methods

Sediment core JM11-FI-19PC was taken at 1179 m water depth (62°49′N; 03°52′W) in April/May 2011 during a cruise with the Norwegian research vessel *Jan Mayen* (Fig. 1).

Magnetic susceptibility was measured every 1 cm before opening of the core using a GEOTEK Multi-Sensor Core Logger (MSCL) coupled with a Bartington magnetic susceptibility meter MS2 (loop). The core liner with an inner diameter of 10 cm was cut into 1-m sections. They were split in two halves, and sampled in 1-cm slices for sediment and diatom analyses.

Total carbon (TC) was measured every 5 cm in a powdered aliquot of the samples with a Leco CS-200. To determine the total organic carbon (TOC) the powdered material was treated with 10% hydrochloric acid (HCl) to remove the carbonates.

Carbon isotopes $\delta^{13}C_{org}$ PDB were measured every 5 cm in a powdered and carbonate-free aliquot of the samples, using a Finnigan MAT Delta-S mass spectrometer equipped with a FLASH elemental analyzer and a CONFLO III gas-mixing system for the online determination of the
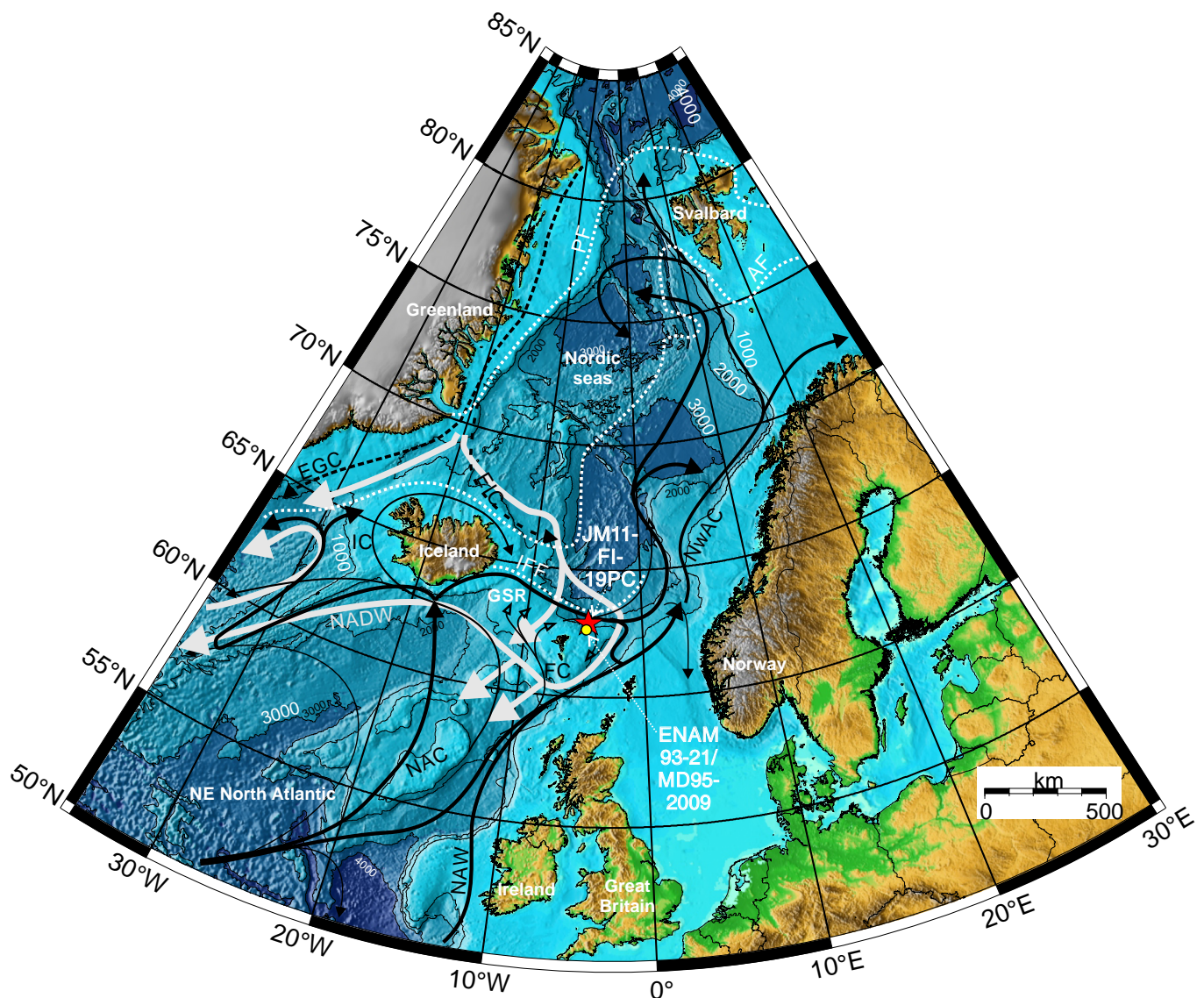
Fig. 1. Map of NE North Atlantic and Nordic seas with position of studied sediment core JM11-FI-19PC (red star) and sediment cores ENAM93-21/MD95-2009 (Rasmussen et al., 1996a,b,c, 1999, 2003a,b) (yellow circle). Main surface and deep currents are based on Hansen and Østerhus (2000) and Orvik and Niiler (2002). Abbreviations: East Greenland Current (EGC), East Icelandic Current (EIC), Faroe Current (FC), Irminger Current (IC), North Atlantic Current (NAC), Norwegian Atlantic Current (NwAC), North Atlantic Water (NAW), North Atlantic Deep Water (NADW), Greenland-Scotland Ridge (GSR). Currents coloured black indicate surface and subsurface warm water currents, dashed black indicate cold surface currents, while light grey indicate cold bottom water currents. Polar Front (PF), Arctic Front (AF) and Iceland-Faroe Front (IFF) are shown in white dashed lines. Bathymetry is given in metres.
The map is modified from Ezat et al. (2014).

carbon isotopic composition. Measurements were conducted at the Alfred Wegener Institute for Polar and Marine Research in Potsdam, Germany. The standard deviation (1σ) is generally better than $\delta^{13}C = \pm 0.15‰$.

The tephra, except tephra 5a-Low/BAS-I (I in Figs. 3, 4), were published in Ezat et al. (2014, 2016) and Hoff et al. (2016). Tephra layers in the upper 685 cm were counted and quantified, whereas tephra layers below 685 cm were detected by visual, microscopical inspection only (Ezat et al., 2016; this study). Previously published AMS ^{14}C dates from cores JM11-FI-19PC (Ezat et al., 2014; Hoff et al., 2016) and ENAM93-21 (Rasmussen and Thomsen, 2004) were (re)-calibrated using the Calib7.04 and Marine13 program (Reimer et al., 2013). We used the standard global reservoir age correction −405 years inherent in the program and the mid-point of the 1σ error interval (Table 1).

For diatom analyses, 1-cm thick samples at every 10 cm were used. In the depth intervals 0–130 (Holocene interglacial and late

deglaciation) and 750–1055 cm (Eemian interglacial) samples at every 5 cm were used to obtain a more detailed comparison of the two interglacials and the transitions to the interglacials. A total of 156 samples were analysed for diatoms.

The preparation method for diatom samples given in Koç et al. (1993) was followed with only few exceptions. Instead of using nitric acid (HNO_3 65%) we used the more gentle hydrogen peroxide (H_2O_2 37%; 10 drops) to remove existing organic matter around the diatom valves. The samples were centrifuged for 3 min at 2000 rounds per minute (rpm) to neutralize them and to remove as much of the clay fraction as possible. Glass vials of known volume were used to store samples at 4 °C. Diatom slides for quantitative analyses were produced as described in Koç Karpuz and Schrader (1990), with Naphrax® with a refraction index of $n = 1.73$, as a mounting-medium. Identification and counting of diatoms were done with a Leitz Aristoplan microscope, ocular Periplan GF 10×, objective NPL-Fluotar 100 × 1.32 oil Phaco 3
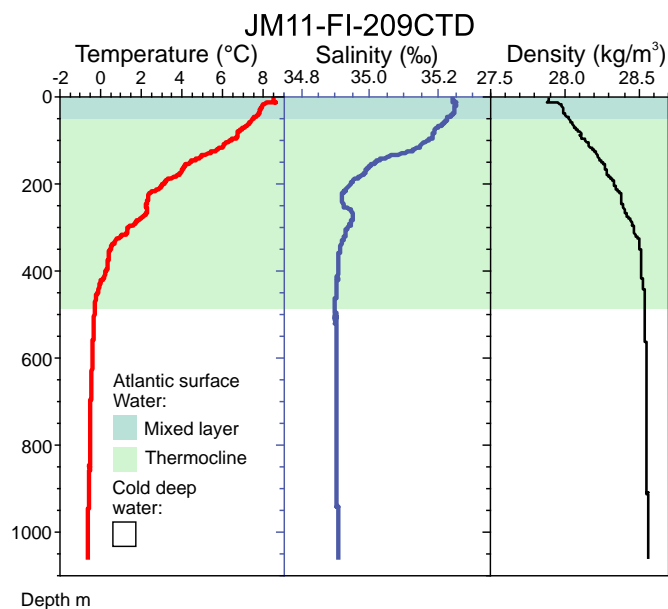
JM11-FI-209CTD

Fig. 2. Conductivity, temperature, depth (CTD) data with identification of water masses taken near core JM11-FI-19PC (JM11-FI-209CTD, 62°45′N, 03°52′W, water depth 1050 m).

(magnification 1000 ×). A sample was considered to contain enough diatoms for quantification, if > 40 diatom valves could be counted within ~350 fields of view (equal to 2 vertical transects). A minimum of 300 diatom valves was counted per sample along the vertical transects. A total of 52 species previously used by Koç Karpuz and Schrader (1990) for establishing a sea-surface-temperature-transfer functions and including additional species added by Andersen et al. (2004) have been the focus of this study as their distribution and environmental requirements are relatively well known. These species constitute about 90% of the species present in the Nordic seas (Koç Karpuz and Schrader, 1990; Koç Karpuz and Jansen, 1992). In addition, three common species not included in this database *Detonula confervacea* (up to 42.9%), *Paralia sulcata* (up to 19.4%), and *Neodenticula seminae* (up to 2.8%) were counted and identified.

Other taxa inclusive resting spores belonging to the subgenus *Chaetoceros* Ehrenberg (*Hyalochaete*) have been counted, but not been identified to species level. A *Chaetoceros* (*Hyalochaete*) resting spore-free basis was chosen, because they often predominate the diatom assemblages and bias reconstructions (e.g., Koç Karpuz and Schrader, 1990; Birks and Koç, 2002; Miettinen et al., 2011). The counting of diatoms followed the procedures of Schrader and Gersonde (1978) and the taxonomic identifications mainly followed Hustedt (1930, 1959), Fryxell and Hasle (1972, 1980), Simonsen (1974), Hasle and Fryxell (1977), Hasle (1978), Syvertsen (1979), Sancetta (1982), Sundström (1986), and Krawczyk et al. (2012).

The raw diatom counts thus include all species present including *Chaetoceros* (*Hyalochaete*) and unidentified species and specimens. The counts were used to calculate the total diatom abundances (concentration = number of valves per gram dry sediment). Concentrations of diatoms (Z) were calculated as follows: $Z = (A \times B) / C \times (D / E) \times F$, where A = total diatom valves (inclusive *Chaetoceros* (*Hyalochaete*)), B = sediment area, C = counted area, D = sample dry weight, E = sample glass volume, F = mounted solution volume. The diatom species abundances are expressed as percentages of specimens of total amount of diatoms counted (on a *Chaetoceros* (*Hyalochaete*)-free basis). Multivariate cluster analysis was performed on the data set using the statistical program CONISS, part of the software package Tilia/Tilia-Graph/TGView 2.0.2 (Grimm, 1991).

The diatom record representing the mixed layer near the sea surface are compared with previously published data of planktic foraminifera (Rasmussen et al., 1996a, 1996c, 1999), which represent the subsurface environment of the thermocline below the mixed layer (Risebrobakken et al., 2011). The diatom results for the last 90 ka are also compared with published sea-ice proxy (IP25) and biomarker data from the same core JM11-FI-19PC (Hoff et al., 2016).

5. Results

The 1109-cm long, continuous and undisturbed sediment record shows generally good preservation of diatoms in the lowermost and uppermost part, whereas valves were strongly fragmented or affected by dissolution in the middle part of the core.

5.1. Chronology

The age model for sediment core JM11-FI-19PC follows Ezat et al. (2014, 2016) and Hoff et al. (2016). Benthic and planktic δ18O records of core JM11-FI-19PC were published by Ezat et al. (2016) in combination with previously described and well-dated tephra layers, AMS 14C dates and the very detailed magnetic susceptibility record. We have correlated core JM11-FI-19PC to the nearby core ENAM93–21/MD95–2009 with identical benthic and planktic δ18O records, AMS 14C dates, tephra layers and magnetic susceptibility patterns (Rasmussen et al., 1996a, 1996c, 1999; Balbon, 2000) (Fig. 3; Table 1). Except for tephra layer FMAZ-I (Faroe Marine Ash Zone), all previously geochemically fingerprinted tephra layers from ENAM93-21/MD95-2009 (e.g., Wastegård and Rasmussen, 2001, 2014; Rasmussen et al., 2003a; Wastegård et al., 2006; Abbott et al., 2014) have been found in JM11-FI-19PC, with the same location in the cores relative to the stable isotopes, AMS 14C dates and magnetic susceptibility (Fig. 3). This close correlation has allowed identification and correlation of interstadials and stadials on a one-to-one basis (Fig. 3). These events were previously identified in JM11-FI-19PC for MIS 3 and MIS 2 by Ezat et al. (2014), for MIS 5a–2 by Hoff et al. (2016), and for MIS 5 by Ezat et al. (2016). In ENAM93-21 they were identified in Rasmussen et al. (1996b, 1996c) and in MD95–2009 by Rasmussen et al. (1999) and Balbon (2000). The Marine Isotope Stage boundaries were identified by comparing with the results of Ezat et al. (2016) (benthic and planktic δ18O records of JM11-FI-19PC), Rasmussen et al. (1999), Lisiecki and Raymo (2005), Sanchez-Goñi and Harrison (2010), Wolff et al. (2010), Abbott et al. (2014) and Railsback et al. (2015).

The age model we use for this study in cores JM11-FI-19PC and ENAM93–21/MD95–2009 was constructed by tying the onsets of the Greenland interstadials and stadials, identified by the combination of δ18O records, AMS 14C dates, the six tephra layers mutual to the marine sediments and the NorthGRIP ice core (e.g., Davies et al., 2008, 2010, 2014; Abbott et al., 2014) and the magnetic susceptibility (see e.g., Rasmussen et al., 1996c, 2003a, 2003b) to the ages of onsets of the interstadials and stadials identified in the ice core (Svensson et al., 2008; Wolff et al., 2010) (Fig. 3). It has been demonstrated in numerous publications that the tephra layers in the NGRIP ice core and marine cores are located at the same levels relative to the various interstadial/stadial events (see Davies et al., 2008, 2010, 2014 and references therein) confirming the reliability of the correlations and age models (Fig. 3). Altogether, JM11-FI-19PC could successfully be correlated to 24 interstadials, known from North Atlantic sediments, and Greenland ice core records, including North Atlantic Heinrich events H11 to H1 (e.g., Heinrich, 1988; Bond et al., 1993).

The final age models of cores JM11-FI-19PC and ENAM93-21/MD95-2009 were calculated by interpolation assuming a constant sedimentation rate between the tie points (Fig. 4). The ages we report are ice core ages ka (GICC05 time scale = kyr before 2000 CE; Svensson et al., 2008; Wolff et al., 2010), unless otherwise specified. The JM11-FI-19PC record is of high resolution with average sedimentation rates of
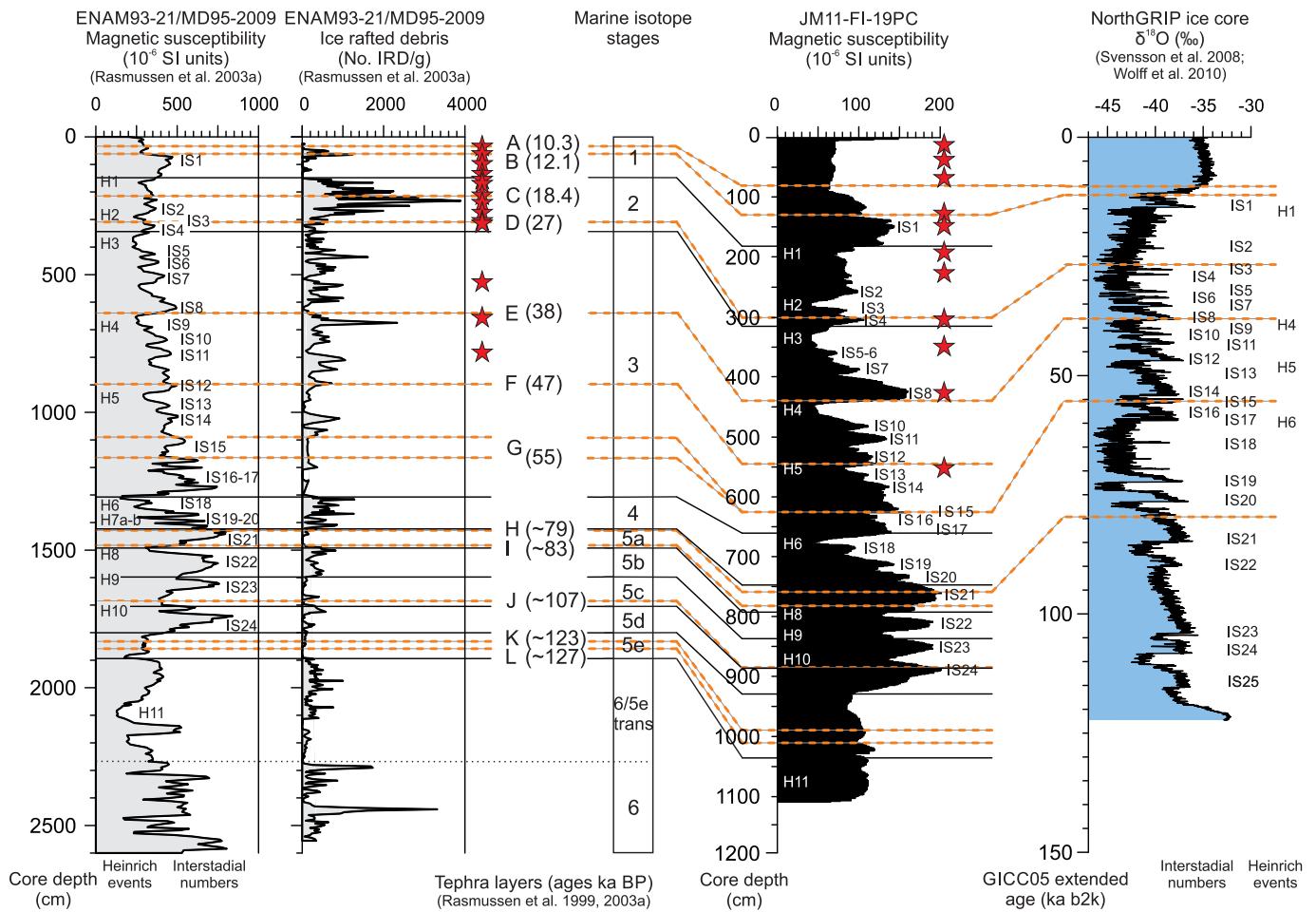
Fig. 3. Stratigraphy and correlation of magnetic susceptibility log of JM11-FI-19PC with magnetic susceptibility, ice rafted debris, tephra layers and marine isotope stages of combined sediment cores ENAM93-21 and MD95-2009 (NE-Faroe slope) from Rasmussen et al. (1996a,b,c, 1999, 2003a,b), Wastegård and Rasmussen (2001, 2014), and Wastegård et al. (2006). Data of JM11-FI-19PC are tied to NorthGRIP ice core time scale (GICC05 ka (= kyr before 2000 CE) (data from Svensson et al., 2008; Wolff et al., 2010). Tephra layers are shown in dashed orange lines denoted A–L with ages in brackets. The position of Heinrich events (H1 − H10) and Interstadial events (IS1–IS24) are indicated. Tephra layers from core JM11-FI-19PC have been identified and published in Ezat et al. (2014, 2016) and Hoff et al. (2016). Legend: A = Saksunarvatn Tephra, B = Vedde Tephra, C = FMAZ-I (Faroe Marine Ash Zone), D = FMAZ-II, E = FMAZ-III, F = FMAZ-IV, G = ASH Zone II, H = 5a-Top/BAS-I, I = 5a-Low/BAS-I, J = 5c-Midt/BAS, K = 5e-Midt/RHY, L = 5e-Low/BAS-IV. Levels of ^{14}C dates are marked by red stars.
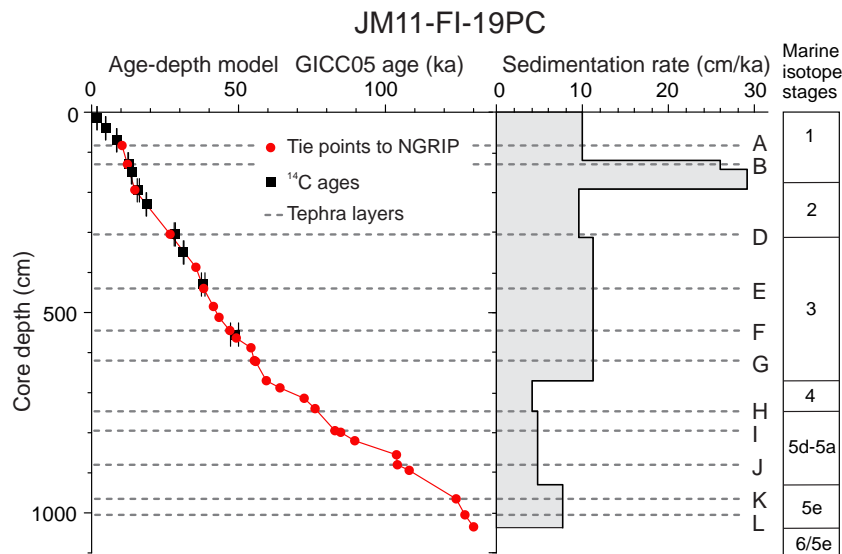
Fig. 4. Age model and sedimentation rates for sediment core JM11-FI-19PC. Tie points to the NorthGRIP ice core and AMS-^{14}C dates are marked. Tephra layers are shown in dashed grey lines denoted A–L, for explanation see legend in Fig. 3. Age scale is in ka (= kyr before 2000 CE).

Table 1
Conventional AMS-^{14}C dates and calibrated ages for cores JM11-FI-19PC and ENAM93-21.

Depth (cm)	Material	Laboratory code	Age (^{14}C yr BP)	Age (cal. yr BP)
Core JM11-FI-19PC:				
15	*N. pachyderma*	UBA-21487	2229 ± 27	1836 ± 40
40	*N. pachyderma*	UBA-21488	4570 ± 32	4659 ± 89
70	*N. pachyderma*	UBA-21489	8083 ± 44	8533 ± 58
130	*N. pachyderma*	UBA-21490	10,905 ± 50	12,458 ± 78
150	*N. pachyderma*	UBA-21894	12,186 ± 53	13,675 ± 127
195	*N. pachyderma*	UBA-21595	13,493 ± 55	15,769 ± 180
230	*N. pachyderma*	UBA-21492	15,786 ± 79	18,748 ± 175
305	*N. pachyderma*	UBA-21493	23,962 ± 166	27,690 ± 127
350	*N. pachyderma*	UBA-21494	27,459 ± 204	31,082 ± 117
430	*N. pachyderma*	UBA-21495	33,614 ± 412	37,434 ± 630
555	*N. pachyderma*	UBA-21496	46,045 ± 2028	48,678 ± 1324
Core ENAM93-21:				
40.5	*N. pachyderma*	AAR-2559	9240 ± 80	10,050 ± 115
67.5	*N. pachyderma*	AAR-2560	11,340 ± 100	12,805 ± 105
100	*N. pachyderma*	AAR-2561	12,140 ± 100	13,590 ± 120
141	*N. pachyderma*	AAR-2562	12,820 ± 110	14,490 ± 270
160	*N. pachyderma*	AAR-1642	13,640 ± 160	15,910 ± 235
175	*N. pachyderma*	AAR-2563	13,650 ± 190	15,920 ± 280
215	*N. pachyderma*	AAR-1643	15,900 ± 170	18,750 ± 170
245	*N. pachyderma*	AAR-1644	18,650 ± 200	22,115 ± 225
280	*N. pachyderma*	AAR-2564	22,420 ± 210	26,235 ± 225
310	*N. pachyderma*	AAR-1645	23,390 ± 310	27,300 ± 290
317.5	*N. pachyderma*	AAR-2565	23,250 ± 190	27,210 ± 210
530	*N. pachyderma*	AAR-2566	30,700 ± 380	34,310 ± 315
660	*N. pachyderma*	AAR-3299	34,650 ± 700	37,755 ± 890
790	*N. pachyderma*	AAR-3300	40,450 ± 1350	43,750 ± 1550
1090	*N. pachyderma*	AAR-3301	47,500 ± 2500	> 50,000

8 cm/ka for the last 130,000 years with lowest rates in MIS 5d–5a and MIS 4 (4.8 and 4.3 cm/ka, respectively) (Fig. 4). The interglacial periods MIS 5e and MIS 1 show rates of 7.6 and 13 cm/ka, respectively. Highest sedimentation rates are found in the deglaciation interval with rates of 30 cm/ka for the Bølling-Allerød interstadials and 26 cm/ka for the Younger Dryas stadial (Fig. 4).

5.2. Distribution of diatoms

The diatom concentration shows a maximum in MIS 5 and MIS 1 (Fig. 5). Diatoms are absent in MIS 4 and of very low concentration in the intervals covering MIS 3 and 2. The intervals with low numbers of diatoms are covered by high resolution data of % TOC and $\delta^{13}C_{org}$, and for the last 90,000 years also by high resolution of IP_{25} and biomarker data (see also Hoff et al., 2016) (Fig. 6a). In total, 15 out of 93 samples with sufficient material for quantification have > 10% unidentified specimens (Fig. 5). Most of these are found in MIS 5d–5a.

The most abundant diatom species throughout the core, excluding *Chaetoceros* (*Hyalochaete*) resting spores, are *Actinocyclus curvatulus* Janisch (0.0–71%), *Shionodiscus oestrupii* (Ostenfeld) Alverson, Kang et Theriot (0.0–47%), *Thalassiosira kushirensis* Takano resting spores (0.0–44%), *Detonula confervacea* (Cleve) Gran (0.0–43%), *Thalassionema nitzschioides* (Grunow) H. et M. Peragallo (0.0–27%), *Thalassiosira antarctica* var. *borealis* Fryxell, Doucette et Hubbard (0.9–26%), *Paralia sulcata* (0.0–19.4%), *Rhizosolenia hebetata* f. *semispina* (Hensen) Gran (0.0–17%), *Thalassiosira nordenskioeldii* Cleve (0.0–17%) and *Thalassiosira angulata* (Gregory) Hasle (0.0–12%). Multivariate cluster analysis (CONISS) identified five diatom assemblage zones (DAZ) (Fig. 5).

5.2.1. DAZ 1 (1109–1025 cm; > 129 ka; MIS 6/5e transition)

Though the preservation of the diatoms is good, there are too few diatoms for quantification below 1055 cm depth. Above 1055 cm, diatom concentrations are low, but increasing to 1.01×10^5 valves g^{-1}

(Fig. 5). The interval is dominated by *A. curvatulus*, which has its maximum relative abundance (up to 71%). Other species present are *Ts. kushirensis* (0.0–16%), *Coscinodiscus marginatus* Ehrenberg (4–9%), *Shionodiscus trifultus* (Fryxell) Alverson, Kang et Theriot (0.6–9%), *Ts. antarctica* var. *borealis* (2–8%), *Bacteriosira bathyomphala* (Cleve) Syvertsen et Hasle (0.3–8%), and *Sh. oestrupii* (0.0–7%) (Fig. 5).

Chaetoceros (*Hyalochaete*) resting spores reach absolute numbers of 787 frustules g^{-1}. The percent TOC is very stable between 0.2 and 0.6%, whereas the $\delta^{13}C_{org}$ signal shows a decreasing trend from −23.3 to −24.2‰ at the lower part and low values at the upper part of the zone (−25.2‰) (Fig. 6a).

5.2.2. DAZ 2 (1025–915 cm; 129–113 ka; MIS 5e–lower 5d ∼ the Eemian)

Similar to the previous zone, the preservation of the diatoms is good. Diatom concentrations increase to a maximum of this zone of 0.57×10^5–1.78×10^5 valves g^{-1} between 124 and 116 ka (980–930 cm) (Fig. 5). DAZ 2 is dominated by *Sh. oestrupii* (4–33%), *Tn. nitzschioides* (4–24%), *Pr. sulcata* (0.8–18.5), *D. confervacea* (0.0–12.5%) and *Ts. angulata* (3–11%). Also present are *Thalassiothrix longissima* (Cleve) Cleve et Grunow (0.4–8%) and *Rh. hebetata* f. *semispina* (0.7–6%). At the boundary between DAZ 1 and DAZ 2, *A. curvatulus* decreases rapidly to 0.3–4% (Fig. 5). *Proboscia alata* (Brightwell) Sundström (0.7–8%), *Thalassiosira lineata* Jousé (1–7%) and *Ts. decipiens* (Grunow) Jørgensen (0.0–5%), though of low relative abundance are persistent in the zone (Fig. 5).

Absolute numbers of *Chaetoceros* (*Hyalochaete*) resting spores are low, but increase to 374 g^{-1} towards the upper part of the zone. The percent TOC increases rapidly to a level of 0.4 to 0.7% at the boundary between DAZ 1 and DAZ 2 (Fig. 6a). The $\delta^{13}C_{org}$ values show a small maximum between 126 and 125 ka (995–980 cm) (∼ −23.5‰), whereas the rest of the interval reveals lower values down to −24.4‰.

5.2.3. DAZ 3 (915–795 cm; 113–87 ka; middle MIS 5d–5b (interstadial 24–22))

The preservation of the diatom shells is poorer compared to earlier. The concentration of diatoms is generally high, but variable (0.14×10^5 to 3.79×10^5 valves g^{-1}). *Shionodiscus oestrupii* (0.0–15%), *Ts. angulata* (2–12%), *Tn. nitzschioides* (0.2–7%), *Rh. hebetata* f. *semispina* (0.0–7%), *Pr. alata* (0.0–3%) and *Tl. longissima* (0.1–2%) decrease in relative abundance. *Detonula confervacea* (1–29%), *Porosira glacialis* (Grunow) Jørgensen (1–6%), *Ts. kushirensis* (7–31%) and *Ts. antarctica* var. *borealis* (5–24%) have higher relative abundance compared to the zone below (Fig. 5).

The part of DAZ 3 that correlates with the lower part of MIS 5c contains the samples with the second highest concentration of diatoms in the core at ∼105 ka (865 cm). The zone also shows the highest absolute numbers of *Chaetoceros* (*Hyalochaete*) resting spores, reaching up to 3667 frustules g^{-1}.

The TOC content decreases towards the upper end of the zone, while the variability increases (0.1–0.5%) (Fig. 6a). The $\delta^{13}C_{org}$ signal displays values around −24‰ before reaching a maximum of −22.2‰ at 102 ka (855 cm) followed by higher levels (∼22.7‰) and a distinct minimum at 88 ka (801 cm) with −25.4‰. The $\delta^{13}C_{org}$ values increase again towards the boundary to DAZ 4.

5.2.4. DAZ 4 (795–100 cm; 87–11 ka; MIS 5a–basal 1 (interstadials 20–1)

DAZ 4 contains, in comparison to all other zones, almost no diatoms (Fig. 5), and the specimens are generally broken and show poor preservation with signs of dissolution and/or diagenetic altering. Except for MIS 5a, very few samples had enough diatoms for quantification. The samples containing diatoms also contain high concentrations of tephra particles. Diatom concentrations range from 0.0 up to 2.43×10^5 valves g^{-1} in the uppermost part of the zone. The most abundant diatom species are *Ts. kushirensis* (8–44%), *D. confervacea*
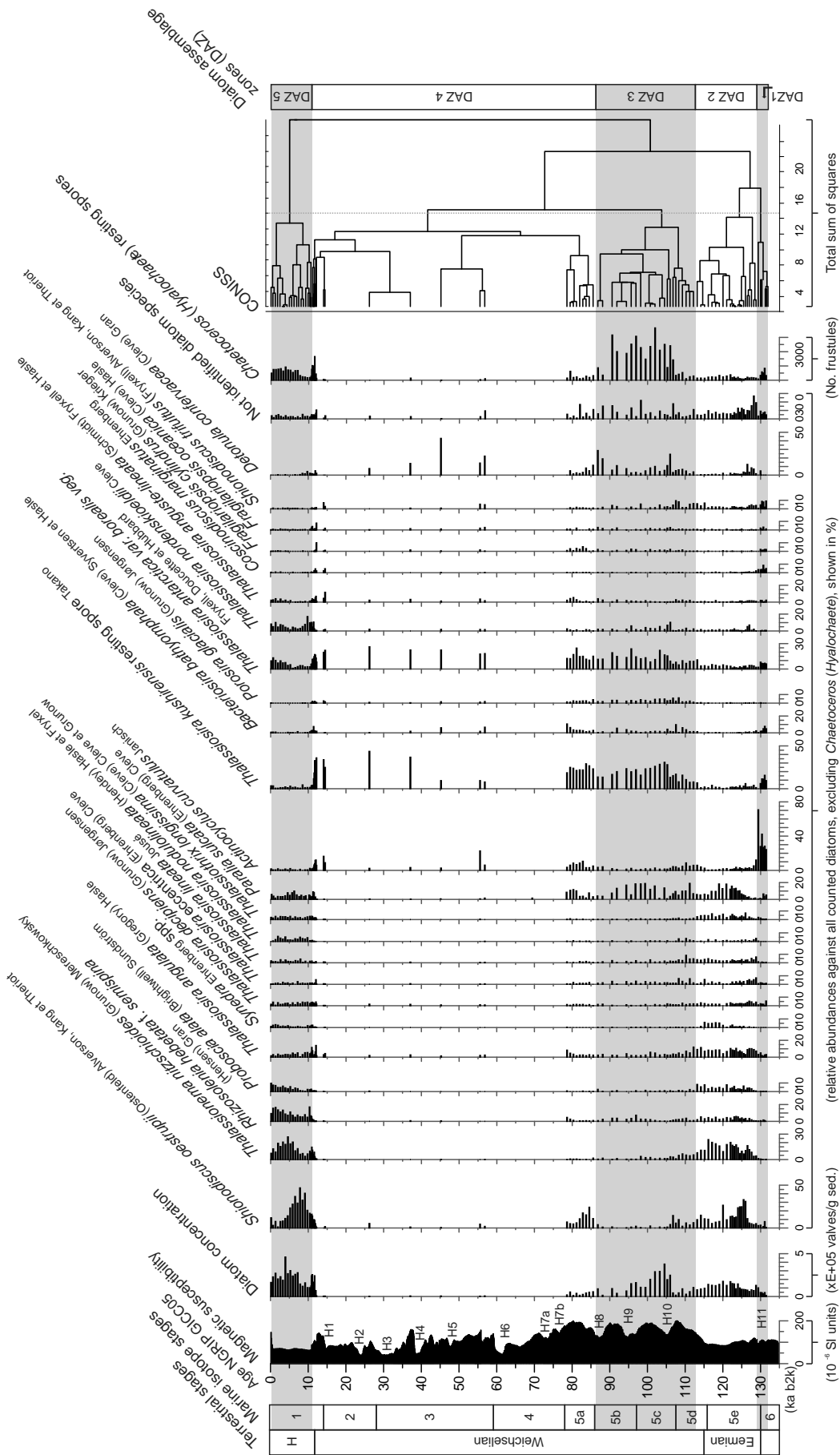
Fig. 5. Relative abundances of diatom species of core JM11-FI-19PC with ≥5% in at least one sample plotted versus ka (= kyr before 2000 CE). Species are presented with species preferring warmer water to the left and colder water to the right. Total diatom concentration (number of valves per gram dry weight sediment on a *Chaetoceros* (*Hyalochaete*) resting spore-free basis) and reconstructed diatom assemblage zones derived from constrained cluster analysis CONISS (DAZ 1–5; right column) are shown. Terrestrial stages and marine isotope stages (MIS) are shown in columns to the left alongside the magnetic susceptibility curve. Abbreviations: Holocene (H).
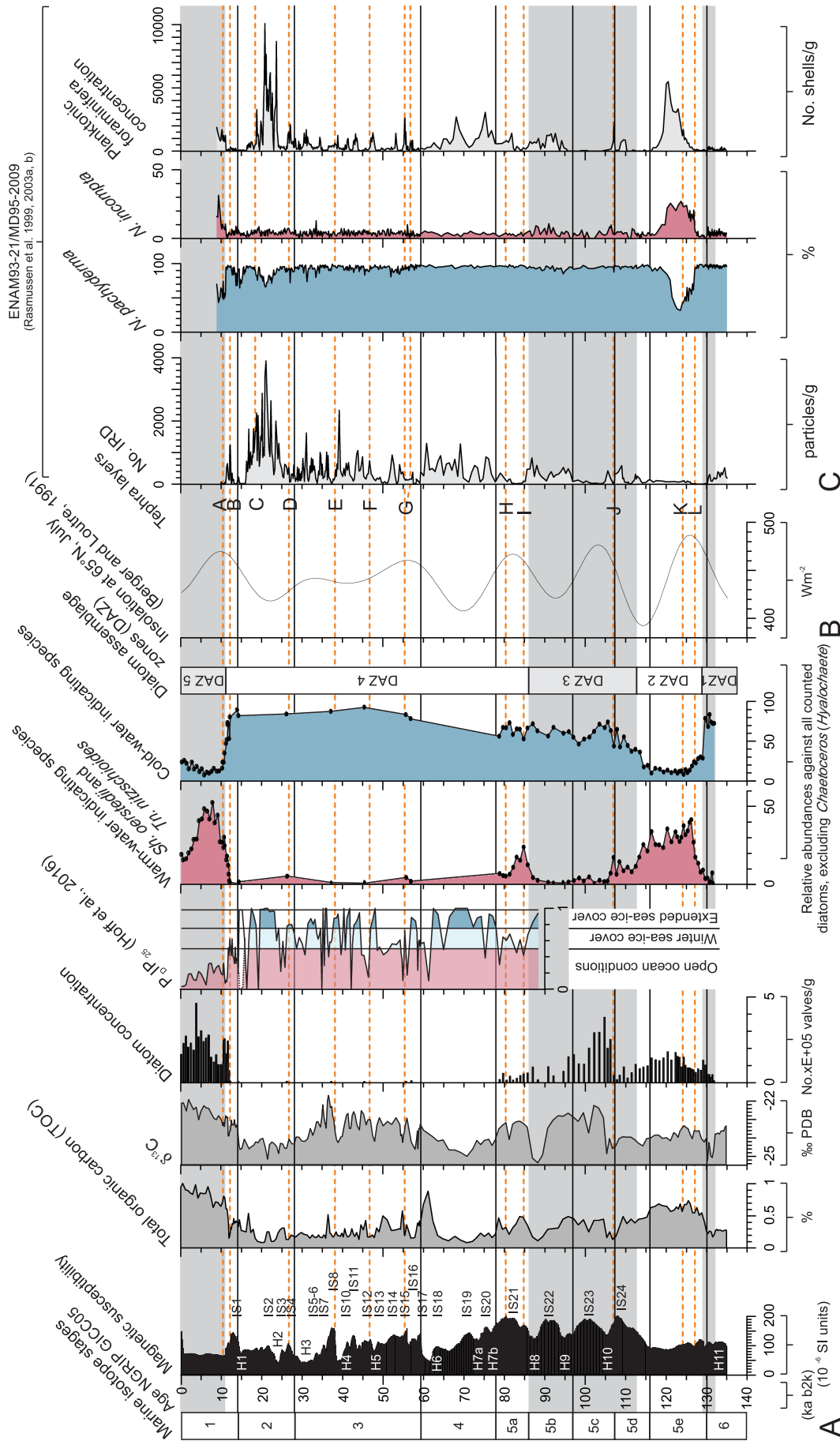
Fig. 6. Comparison of diatom and foraminiferal data plotted versus ages (ka = kyr before 2000 CE). a) records of core JM11-FI-19PC of magnetic susceptibility, % TOC, δ¹³C$_{org}$, diatom concentration (number valves per gram dry weight sediment), P$_B$IP$_{25}$-index as indicator for degree of sea-ice cover, relative abundance for the two dominant warm-water indicating diatom species *Shionodiscus oestrupii* and *Thalassiosira nitzschioides* added together and all cold-water indicating species added together; b) insolation curve for 65°N based on data from Berger and Loutre (1991) c) correlation to previously published foraminifera and IRD data from sediment core ENAM93-21/MD95-2009 (Rasmussen et al., 1996a,b,c, 1999, 2003a,b). Tephra layers are shown in dashed orange lines denoted A–L, for explanation see legend in Fig. 3. Cold-water indicating species added together are: *Actinocyclus curvatulus*, *Actinocyclus octonarius* (Syn.: *Actinocyclus curvatulus*, *Actinocyclus octonarius* (Syn.: *Actinocyclus ehrenbergi*), *Asteromphalus robustus*, *Bacteriosira bathyomphala*, *Coscinodiscus asteromphalus*, *Coscinodiscus marginatus*, *Coscinodiscus oculus-iridis*, *Detonula confervacea*, *Fragilariopsis cylindrus*, *Fragilariopsis oceanica*, *Nitzschia angularis*, *Nitzschia atlantica* (or: *Nitzschia pungens* var. *atlantica*), *Porosira glacialis*, *Rhizosolenia hebetata* f. *hebetata*, *Thalassiosira anguste-lineata*, *Thalassiosira antarctica* var. *borealis*, *Thalassiosira hyalina*, *Thalassiosira kushirensis*, and *Thalassiosira pacifica*.

(0.0–43%), *Ts. antarctica* var. *borealis* (8–26%) and *A. curvatulus* (2–23%). *Thalassiosira anguste-lineata* (Schmidt) Fryxell et Hasle (0.3–12%), *Fragilariopsis cylindrus* (Grunow) Krieger (0.0–10%) and *F. oceanica* (Cleve) Hasle (0.0–8%) show their highest percentages of the record. *Chaetoceros* (*Hyalochaete*) resting spores show absolute numbers of 3–1661 g^{-1}, reaching highest values of this zone right before the transition to DAZ 5.

The percent TOC is low in MIS 4, but shows a high peak (0.9%) at 61 ka (676 cm) (Fig. 6a). In MIS 3 and MIS 2, % TOC varies on millennial scale. After a decrease of δ^{13}C$_{org}$ values at the beginning of DAZ 4, the values increase towards a maximum of ~ − 21.7‰ at about 35 ka (411 cm). This is followed by another decrease towards DAZ 5.

5.2.5. DAZ 5 (100–1 cm; < 11 ka; MIS 1–Holocene)

The diatom preservation is good. DAZ 5 is characterized by the highest diatom concentrations in the record (1.03–4.61 × 10^5 valves g^{-1}) (Fig. 5). *Shionodiscus oestrupii* (1–47%) and *Pr. alata* (0.30–10%) show their maximum relative abundance throughout the core, whereas *Tn. nitzschioides* (4–27%), *Rh. hebetata* f. *semispina* (3–17%), *Ts. nordenskioeldii* (2–17%), and *Ts. antarctica* var. *borealis* (0.9–13%) present intermediate relative abundances.

Chaetoceros (*Hyalochaete*) resting spores (170–1024 g^{-1}) are overall dominant as in DAZ 1–3. The percent TOC increases steadily throughout the zone (Fig. 6a). The δ^{13}C$_{org}$ values show the same increasing trend with values between − 23.4 and − 21.9‰.

6. Discussion

6.1. Interpretation of diatom floras and comparison with planktic foraminiferal distribution

The diatom record in core JM11-FI-19PC of the past ~130,000 years indicates pronounced variations in surface water conditions over the central Northern Faroe slope in the southern Norwegian Sea (Figs. 5, 6a). The diatom assemblages reflect changes in temperature, salinity, sea-ice cover and productivity of the surface water as we discuss below.

6.1.1. DAZ 1, MIS 6/5e transition, > 129 ka

The dominant species *A. curvatulus* with maximum relative abundance in the record (Fig. 5) is a widespread (cosmopolitan) species, which occurs attached to sea-ice in the Arctic (Hasle and Syvertsen, 1997) and subarctic regions (Witkowski et al., 2000). It is also common in the Sea of Okhotsk, where the surface water is cold, ice covered in winter, highly stratified and of lower salinity (salinities of 32–33‰) (Barron, 1992). The presence of the high-latitude species *Ts. antarctica* var. *borealis*, *Sh. trifultus*, *F. cylindrus* and *F. oceanica* preferring colder and fresher Arctic water masses (e.g., Ramsfjell, 1960; Kanaya and Koizumi, 1966; Jousé et al., 1971; Sancetta, 1982; Williams, 1986; Koç Karpuz and Schrader, 1990; Koç Karpuz and Jansen, 1992; Hasle and Syvertsen, 1997; Gersonde and Zielinski, 2000; Krawczyk et al., 2012; Oksman et al., 2019) also point to colder conditions with seasonal sea-ice cover and thus stronger influence of meltwater and the EIC. Another high-latitude species *B. bathyomphala* has been reported from pack ice, the ice margin and its underlying sediments (e.g., Horner, 1982, 1985; Sancetta, 1982; Williams, 1986; Koç Karpuz and Schrader, 1990; Oksman et al., 2019).

The species *C. marginatus* (Fig. 5) belongs to the Arctic-Norwegian Water Mixing assemblage of Koç Karpuz and Schrader (1990), which generally is found in slightly colder water masses than at present. *Shionodiscus oestrupii* associated with the warmer North Atlantic Water masses with temperature > 8 °C and salinities > 35.3‰ (previously *Ts. oestrupii*; Maynard, 1976; Koç Karpuz and Schrader, 1990) appears in relatively low percentages (Fig. 5). *Thalasiossira kushirensis* has not previously been reported from off the Faroe Islands and Iceland, most likely because it has been confused with resting spores of *Thalassiosira gravida* Cleve or *Ts. antarctica* var. *borealis*. Krawczyk et al. (2012) and

Weckström et al. (2014), show that *Ts. kushirensis* resting spores mostly occur in cold and more Arctic conditions.

In general, the % TOC content in marine sediments is related to the surface productivity and organic matter preservation (e.g., Emerson and Hedges, 1988; Calvert and Pedersen, 1992; Canfield, 1994). The % TOC is low as is the concentration of diatoms, together indicating low productivity rather than dissolution effects (Figs. 5, 6a). The δ^{13}C$_{org}$ signal is used to distinguish between different sources of the bulk organic matter (Meyers, 1994, 1997, 2003). Marine organic matter typically shows δ^{13}C$_{org}$ values between − 22‰ and − 20‰ (Meyers, 1994), terrestrial C$_4$ plants ~ − 14‰ (Meyers, 1997), and terrestrial C$_3$ plants between − 28‰ and − 26‰ (Meyers, 1994, 1997). The bulk organic matter in core JM11-FI-19PC is likely a two-component mixture of marine phytoplankton (mainly diatoms) and terrestrial C$_3$ plants. The decrease in δ^{13}C$_{org}$ values, while % TOC stays nearly constant could be related to an increased input of terrestrial organic matter (Fig. 6a). This applies especially for the top of DAZ1, where δ^{13}C$_{org}$ values reach − 25.2‰.

The diatom assemblages together with relatively high concentrations of IRD and very high percentages of the polar planktic foraminiferal species *Neogloboquadrina pachyderma* (Bé and Tolderlund, 1971; Carstens and Wefer, 1992) in the same time interval in core ENAM93–21/MD95–2009 (Fig. 6c), point to a cold and stratified water column with relatively fresher surface water and seasonal sea-ice cover. The concentration of both diatoms and planktic foraminifera is low, most likely indicative of the extensive ice cover and low nutrient and food availability as presently seen behind the Polar Front (e.g., Koç Karpuz, 1989) and with significantly reduced influence of Atlantic surface water (Fig. 6a,c).

6.1.2. DAZ 2, MIS 5e–lower 5d (Eemian), 129–113 ka

DAZ 2 correlates with the Eemian comprising the middle to upper MIS 5e and lower 5d (Figs. 5, 6).The three species *Sh. oestrupii*, *Tn. nitzschioides* and *Ts. angulata* shows high relative abundances, while the cold and cool water indicating species from DAZ 1 show low relative abundances (Fig. 5). In the Nordic seas, *Ts. angulata* belongs to the Norwegian Atlantic Current assemblage associated with Atlantic surface Water (Koç Karpuz and Jansen, 1992). This points to warmer surface conditions compared to the previous zone (Fig. 5). *Detonula confervacea*, a species most common at temperatures below 1 °C and a salinity range of 15–30‰ (Smayda, 1969), is abundant in the lowermost part and indicates that colder and fresher surface water still influenced the core site until ~126 ka (Fig. 5). *Shionodiscus oestrupii* increases to a maximum at 126–124 ka followed by a decline towards the upper part of the zone, interrupted by an increase at 121–120 ka and at ~115 ka. Since the species prefers warm North Atlantic water masses, the first peak points to the warmest surface conditions within this zone followed by two warm events (Fig. 5). In modern surface sediments *Sh. oestrupii* together with *Tn. nitzschioides* are most abundant south and southwest of Iceland in the direct flow path of the warm Irminger Current (Jiang et al., 2001, 2002; Knudsen et al., 2004) (Fig. 1). Together they indicate warmer surface water than at present for most of the Eemian (Fig. 5). The diatoms indicate an increased inflow of warm and saline Atlantic surface water of the Faroe Current, while the cold EIC weakened. *Thallasiosira nitzschioides* and *P. alata* increase in relative abundance (Fig. 5). They are associated with colder, more diluted Atlantic waters with temperatures > 3 °C and salinities > 34.9‰ (Koç Karpuz, 1989), which in combination with the decreasing trend of *Sh. oestrupii* suggests a general cooling and decrease in salinity towards the upper part of DAZ 2. The taxa *Rh. hebetata* f. *semispina* and *Ts. nordenskioeldii* both show increasing relative abundance in the Eemian interglacial, but lower than in the Holocene (Fig. 5). They prefer the mixed Atlantic and Arctic Water masses found between the Iceland-Faroe Front and the Arctic Front (e.g., Koç Karpuz and Schrader, 1990; Jiang et al., 2001; Witon et al., 2006), which suggests the Iceland-Faroe Front probably was poorly developed or absent during the Eemian in

contrast to today and most of the Holocene (see below).

Percent TOC values are high and diatom concentrations peak in the middle part of the Eemian interval (Fig. 6a). This indicates a significant increase in biological productivity compared to both the pre-Eemian zone DAZ 1 and the lowermost part of the Eemian interval (Fig. 6a,c). The $\delta^{13}C_{org}$ values show a rather stable signal with values around −24‰, which indicates a continuous influence of terrestrial organic matter (Fig. 6a). The reason could be a steady freshwater runoff from the Faroe Islands due to the higher temperatures.

Low concentration of IRD together with a sudden increase in percentage of the subpolar planktic foraminiferal species *Neogloboquadrina incompta* (previously *N. pachyderma* dextral) (Darling et al., 2006) just above the lowermost tephra layer (5e-Low/BAS-IV; Fig. 3) in MIS 5e also clearly reveal a signal of warmer water (Fig. 6c). As this foraminiferal species represents subsurface conditions, it is assumed that the comparatively late foraminiferal signal of warmer water indicates the Atlantic water masses during the early Eemian were restricted to the surface with a shallower and steeper thermocline than today (Fig. 2). At 126 ka, the thermocline became deeper and warmer pointing to stronger influence of warm Atlantic surface water from the Faroe Current than in modern times (Fig. 6c). This indicates that the Polar and Arctic fronts were farther northwest of the core site than at present. The cooling and increase in productivity compared to the early Eemian indicates approach of the Arctic Front and colder, more fertile Arctic surface waters. The warm water signal of the planktic foraminifera disappears suggesting the Faroe Current had weakened and the thermocline became steeper and shallow again (Fig. 6c).

6.1.3. DAZ 3, MIS 5d–5b (interstadial 24–22), 113–86 ka

Through MIS 5d and 5c, the warm water species *Sh. oestrupii*, *Ts. angulata* and *Tn. nitzschioides* decrease in relative abundance, while the cold and cool water indicating species *Ts. antarctica* var. *borealis*, *Ts. kushirensis* and *D. confervacea* become increasingly dominant (Fig. 5). These trends indicate a steady cooling of the surface water and weakening inflow of Atlantic surface water towards MIS 5a, except for a short reversal at 107–106 ka (Figs. 5, 6a). The influence of colder water masses reached a climax at Heinrich Event H10 at about 106–105 ka when *P. glacialis*, a species associated with sea ice (Koç Karpuz and Schrader, 1990) also became a persistent part of the flora, although of low relative abundance (Fig. 5).

The diatom assemblage of the main part of MIS 5c–b shows high relative abundances of *Ts. antarctica* var. *borealis* and *Ts. kushirensis* (Fig. 5). *Thalassiosira kushirensis* (as *Ts. gravida* spore) and *Ts. antarctica* var. *borealis* (part of *Ts. gravida* vegetative) both belongs to the 'Arctic Water assemblage' of Koç Karpuz and Schrader (1990), which prefers the fertile Arctic surface Water with salinities of 34.7–34.9‰ and temperatures from freezing to 8 °C. Together, they indicate that the EIC continued to bring in colder Arctic surface water. Further, *Chaetoceros* (*Hyalochaete*) resting spores become very abundant in the middle part. The subgenus is associated with high phytoplankton productivity and strong stratification from meltwater (Crosta et al., 1997), which is presently found at the Arctic Front and the outer part of the seasonal sea-ice covered Arctic surface Water. At the end of MIS 5b (top DAZ 3), correlating with Heinrich Event H8, *D. confervacea* reaches a new maximum in relative abundance indicating colder and more melt-water influenced surface conditions.

The diatom concentration shows one large maximum in MIS 5c (Fig. 6a). The $\delta^{13}C_{org}$ values show a trend of stronger terrestrial input of organic matter in MIS 5d, followed by significantly higher concentrations of marine organic matter (phytoplankton) in MIS 5c and most of 5b (Fig. 6a). The peak in the $\delta^{13}C_{org}$ at 102 ka (−22.2‰) is most likely caused by higher diatom productivity, while the minimum in Heinrich Event H8 at 88 ka (−25.4‰) appears to be associated with lower phytoplankton productivity (lower absolute diatom concentrations) and relatively higher input of terrestrial C_3 plants. However, the phytoplankton productivity seems mostly to have been moderate, which

according to the studies of Belt and Müller (2013) and Hoff et al. (2016), and in agreement with the diatom flora, suggests the core site now was located closer to the Polar Front. The minimum in phytoplankton productivity in H8 in MIS 5b coincide with an IRD maximum, where also all the warm water species almost disappear (Figs. 5, 6a,c). This indicates that the area experienced extended or near-perennial sea-ice cover and low influence of Atlantic surface water.

In the ENAM93–21/MD95–2009 record cold-water is indicated by constantly high relative abundance of *N. pachyderma* (Fig. 6c). The concentration of IRD is higher than during the Eemian, but still low (except in MIS 5b) compared to the fairly strong cooling signal of the diatoms and foraminifera. It is likely that there was a different wind regime or a delay in the IRD signal as the glaciers needed time to build up after the Eemian.

During MIS 5d it is also probable that the high relative abundances of the warm-water loving *Sh. oestrupii*, and high relative abundance of the polar foraminifera *N. pachyderma*, is caused by their different habitats (Figs. 5, 6a,c). A weak inflow of warmer Atlantic water in MIS 5d and 5c might have caused the thermocline to become shallower and steeper.

One distinct difference in the diatom/foraminifera signals is revealed in MIS 5c. This subinterval comprises the highest diatom concentrations of DAZ 3 (Fig. 6a), whereas, after a sharp peak at the beginning of this interval, it also comprises the lowest planktic foraminiferal concentration of the whole record (Fig. 6c). It is likely that the high organic productivity in the fertile Arctic surface water increased the supply of organic material to the sea floor and eventually led to dissolution of the foraminiferal specimens (see e.g., Zamelczyk et al., 2012 and references therein).

6.1.4. DAZ 4, MIS 5a–2 (interstadials 21–1), 86–11 ka

The interval is characterized by an almost complete lack of diatoms except in MIS 5a and the base of MIS 1 (Fig. 5). Here, *Sh. oestrupii* reappears, indicating warmer surface conditions and inflow of Atlantic water. Continued high relative abundance of *Ts. antarctica* var. *borealis* and *Ts. kushirensis* indicate a persistent influence of colder water, which together with presence of *P. glacialis* and an increase in relative abundance of *A. curvatulus* and *F. cylindrus* indicates presence of a thin layer of meltwater at the surface and continued seasonal sea-ice cover.

In MIS 4–2, only a few samples contained enough diatoms for quantification. The poor preservation of diatom shells, including partly dissolved and/or recrystallized valves indicates, that in addition to very low productivity (see below), dissolution also decreased the concentration of diatoms in the sediments. The dominance of *Ts. antarctica* var. *borealis*, *Ts. kushirensis* and *D. confervacea*, and the nearly complete absence of warm water species above MIS 5a, indicate that the central northern Faroe slope was strongly influenced by cold water of the EIC and close to or even north of the Polar Front most of the time (Fig. 5). This is supported by IP_{25} and biomarker data showing mostly permanent to near-permanent sea-ice cover (Fig. 6a).

The deglaciation comprising the Bølling-Allerød interstadials and the Younger Dryas stadial has the maximum time resolution of the record (Figs. 4, 6, 7). Most of this interval is unfortunately almost devoid of diatoms, while the IP_{25} and biomarker record indicates seasonal sea-ice cover (Figs. 6a, 7). At 12.2 ka concomitant with deposition of the Vedde tephra, diatom concentration increases steeply, first dominated by cold water species, including *A. curvatulus*, *Ts. anguste-lineata*, *F. cylindrus* and *F. oceanica* indicating continued presence of seasonal sea ice (supported by the IP_{25} and the biomarker record; Figs. 6a, 7) and *Chaetoceros* (*Hyalochaete*) pointing to a stratified water column (Fig. 5). The interval dominated by cold-water species represents the Younger Dryas cooling event (Fig. 7). The high concentration of diatoms shows, that despite it being a cooling event, the extensive sea-ice cover characterising the area during most of the Weichselian did not re-establish as also shown by the sea-ice proxies of Hoff et al. (2016) in Figs. 6a and 7.
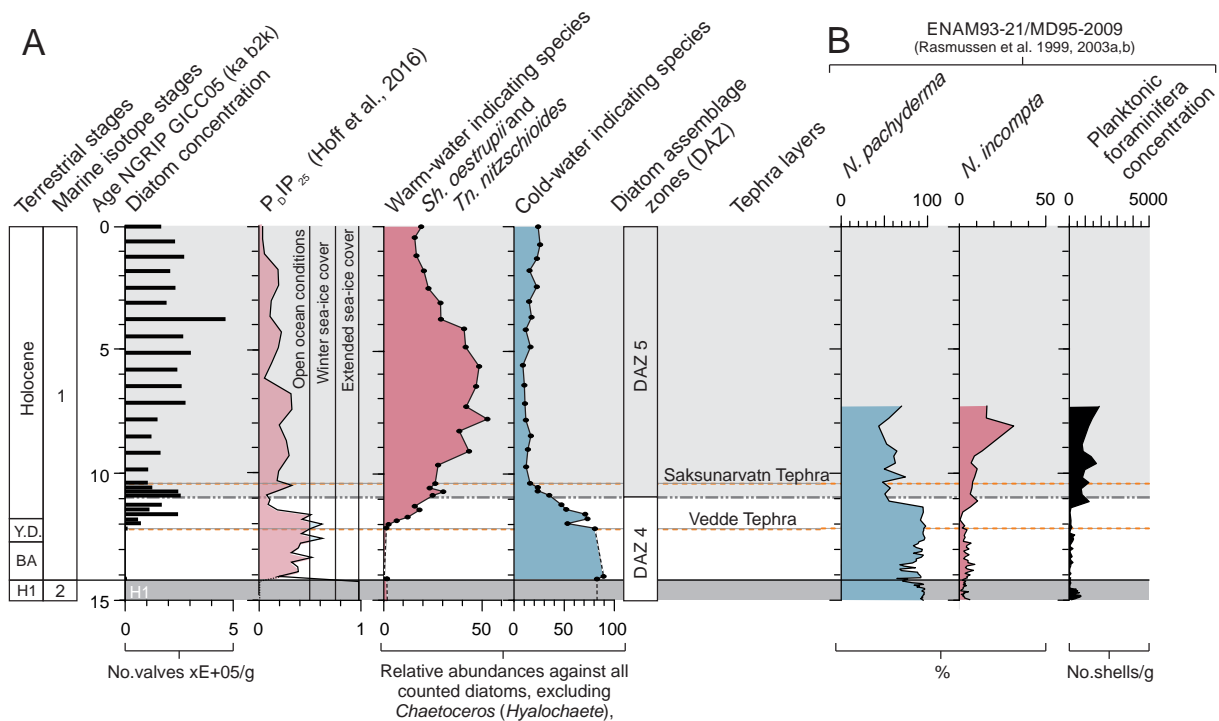
Fig. 7. Details of the last 15,000 years of cores JM11-FI-19PC and ENAM93–21. H1 is marked by dark grey bar. See Fig. 6 for explanation of other symbols.

The % TOC is generally low and with small fluctuations, but in parts still high compared to the low concentration of diatoms (Fig. 6a). The $\delta^{13}C_{org}$ record shows a relatively high amount of marine organic matter in MIS 5a, though the relatively lower % TOC and diatom concentration indicate the phytoplankton productivity in reality was lower than earlier and the relatively high $\delta^{13}C_{org}$ values partly are a result of lower supply of terrestrial organic particles. Between Heinrich events H6 and H3 in lower MIS 3, the relatively high $\delta^{13}C_{org}$ values support the assumption that a large part of the TOC is derived from phytoplankton productivity. Here, the % TOC is higher when sea-ice cover is reduced and vice versa, indicating millennial scale changes in productivity, with slightly higher productivity during interstadials (Fig. 6a). The MIS 4 and DAZ 4 part above Heinrich event H3 (upper MIS 3 and MIS 2) show a stronger terrestrial organic signal, which combined with minimum % TOC indicate extremely low phytoplankton productivity rather than increased input of terrestrial organic matter in line with the more extensive sea-ice cover indicated by the IP₂₅ and biomarker data (Hoff et al., 2016) (Fig. 6a). This, together with the continuously high percentages of the planktic foraminiferal species *N. pachyderma* seen in core ENAM93–21/MD95–2009 corresponds well with an interpretation of cold surface water close to the Polar Front, where the open-water season most of the time was too short for any real phytoplankton productivity (Fig. 6c). The signal of increased Atlantic water from the diatoms in MIS 5a is not observed for the planktic foraminifera, indicating a steep and shallow thermocline and cold subsurface water. The content of IRD is nearly zero in MIS 5a supporting the interpretation of incoming Atlantic water from the Faroe Current. The IRD in the part of DAZ 4 that correlates with MIS 4, upper MIS 3 and MIS 2, shows peaks of medium to high values in many stadials and Heinrich events, and correlating with increased sea-ice cover as indicated by the IP₂₅ and biomarker data (Fig. 6a,c). This supports the interpretation of presence of rather cold water close to the Polar Front (see also Rasmussen et al., 1996a, 1996c).

Similar to the Eemian, we see a significant delay in the warm signal of the planktic foraminifera compared to the diatoms in lower MIS 1 (Figs. 6a,c, 7). The foraminifera indicate warming by showing a decrease in relative abundance of *N. pachyderma* and increase in *N.*

incompta at ~11.2 ka in the early Holocene. The first warming signal from the diatoms already came during the Younger Dryas at ~12 ka. This indicates that when the Faroe Current started to bring in warm Atlantic surface water, the thermocline was shallower and steeper. Slightly before 11 ka the inflow abruptly strengthened and warmed the subsurface layers.

6.1.5. DAZ 5, middle and upper MIS 1 (Holocene), < 11–0 ka

The lower boundary of DAZ 5 marks where the warm water indicating diatom species become a significant part of the assemblage from ~11 ka in the early Holocene (Fig. 5). DAZ 5, comprising most of the Holocene interglacial, is very similar to DAZ 2, the Eemian interglacial (Figs. 5, 6a, 7). One difference is found in the lowermost and again in the upper part of the zone, where *Rh. hebetata* f. *semispina* and *Ts. nordenskioeldii* become relatively abundant. These taxa prefer the mixed Atlantic and Arctic Water masses found between the Iceland-Faroe Front and the Arctic Front, indicating that in response to the Holocene influx of warmer surface waters and the north-western retreat of the Arctic Front, the Iceland-Faroe Front had developed and the EIC was stronger than during the Eemian. In the lower middle part of the Holocene, *Sh. oestrupii* shows its highest relative abundances. Also *Tn. nitzschioides* is abundant (Fig. 5). Together with very low relative abundances of *Ts. antarctica* var. *borealis* and *Ts. kushirensis*, this points towards the warmest surface conditions in the whole record and thereby a strong influence of Atlantic water and the Faroe Current. It also means all the oceanic fronts had moved north of the core site. This interpretation is supported by the highest percent TOC and $\delta^{13}C_{org}$ values (highest phytoplankton productivity) as well as the highest diatom concentrations of the record, and an almost lack of IRD, suggesting year-round sea-ice free conditions (Fig. 6a,c). In contrast to the diatoms the foraminifera in core ENAM93–21 indicate the Eemian had the highest water temperatures suggesting a deeper and warmer thermocline in the Eemian than in the early-mid Holocene) (Figs. 6a,c). The decrease in abundance of *Sh. oestrupii* as well as the increase in relative abundance of *Ts. antarctica* var. *borealis* in the upper part of the Holocene probably reflects the late Holocene cooling. In core ENAM93-21 the upper Holocene is believed to be missing, but the planktic

foraminifera show a cooling signal at the very top (Figs. 6c, 7).

6.2. Comparison with other studies

Over the past four decades a high number of studies investigating the last 150,000 years of oceanographic and climatic changes in the North Atlantic and Nordic seas have been published (e.g., Kellogg et al., 1978; Streeter et al., 1982; Labeyrie and Duplessy, 1985; Haake and Pflaumann, 1989; Fronval and Jansen, 1996; Fronval et al., 1998; Rasmussen et al., 1996c, 1999). These studies are based on a wide range of proxies, but mainly on foraminifera and/or stable isotopes. Most studies based on diatoms are focused on the Eemian or the Holocene interglacials or short parts of the Weichselian. This is the first diatom record comprising the entire last ~130,000 years from the Nordic seas.

In their foraminifera-based study Fronval and Jansen (1997) concluded that during marine isotope stage 5e, comprising the lower and middle Eemian, the sea surface temperatures of the Iceland Sea was higher by > ~5 °C. In accordance with our interpretation of warmer surface waters and a stronger influence of the Faroe Current compared to the EIC within this entire period, Fronval and Jansen (1997) and Fronval et al. (1998) suggested that the Arctic Front was located more north-westerly, while the Atlantic water had an enhanced influx to the Iceland-Greenland Sea and the EGC was weaker. Both the Irminger Current and Faroe Current originate from the warm NAC. In addition, the missing signal of a developed Iceland-Faroe Front indicates that the surface water masses were more homogenous during the Eemian with weaker temperature and salinity gradients than today (Fig. 1), which again support the hypothesis that the EGC/EIC had weakened.

In two studies from the main path of the Norwegian Atlantic Current (NwAC), Bauch et al. (2011) from off mid-Norway and Zhuravleva et al. (2017) from the Fram Strait at western Svalbard, found that the warmest interval of the Eemian occurred at 124–114 ka with a short cold event at about 120 ka. The cold event was also recorded by Fronval et al. (1998) from the central Nordic seas. In our study the interval centred at 120 ka coincides with peak influence of warm, saline Atlantic surface water from the Faroe Current (Fig. 5). It therefore seems that the flow of Atlantic water was deflected towards the Faroe Islands. This supports the suggestion by Bauch et al. (1999, 2011), that much of the Atlantic surface water flowed westward and remained at mid-northern latitudes, when the main flow of the NwAC weakened.

A decrease in sea surface temperature was reported in numerous studies of the late part of MIS 5e, where the northern North Atlantic cooled in response to a decrease in June insolation at 65°N (Fig. 6b), while the mid-latitudes were still warm (e.g., Cortijo et al., 1994; Fronval and Jansen, 1997; McManus et al., 2002; Tzedakis, 2005; Alonso-Garcia et al., 2011; Capron et al., 2014). At the glacial inception, the ocean circulation in the Arctic and subpolar North Atlantic probably had undergone a reorganization, with enhanced sea-ice export through the EGC during winters (Born et al., 2010; Alonso-Garcia et al., 2011). The increasing amount of sea ice caused increased albedo and isolation of the ocean surface water from the atmosphere and, as a consequence, annual sea surface temperature decreased at high latitudes (Crucifix and Loutre, 2002; Alonso-Garcia et al., 2011). At the start of MIS 5a, the diatom signal shows a peak in *Sh. oestrupii* and renewed influx of Atlantic surface water in agreement with the findings of Bauch et al. (2012) (Fig. 5). Higher concentrations of the foraminiferal specimens indicated increased productivity in line with the diatom data (e.g., Belanger, 1982; Fronval and Jansen, 1997; Fronval et al., 1998; Rasmussen et al., 1999) (Fig. 6c).

The diatom-based sea-ice proxy IP_{25} together with other phytoplankton proxy data for the last 90 ka (Hoff et al., 2016) show that there is a very good agreement between absence of diatoms and extensive to perennial sea-ice cover (Fig. 6a). In MIS 3–basal MIS 1, the samples with enough diatoms for quantification are from depth intervals representing the warmest interstadials (IS 16, IS 15, IS 12, IS 8, IS 3–4 and IS 1) with the least sea-ice cover. The study of Hoff et al. (2016)

indicates permanent to near-perennial sea-ice cover north of the Faroe Islands during most of upper MIS 3 and MIS 2 including the Last Glacial Maximum (c. 24–19 ka) and similar to results from the Svalbard margin (Müller et al., 2009; Müller and Stein, 2014) (Fig. 6a).

There is a good agreement between the present study and the diatom-based palaeoceanographic studies by Koç Karpuz and Jansen (1992), Koç et al. (1993), and Berner et al. (2011) of the Nordic seas for the last 14 ka. In the Bølling-Allerød interstadials and Younger Dryas stadial the deposits yielded very low diatom concentrations, which indicate unfavourable surface conditions for diatom production, caused by cooling from melting of the Scandinavian ice sheet prior to the establishment of the warm NwAC. The Younger Dryas cold stadial lasted from ~12.9 to 11.7 ka (Liu et al., 2012). Sea surface temperatures dropped 6 °C, bringing Arctic conditions to Norway (Koç Karpuz and Jansen, 1992; Koç et al., 1993; Birks and Koç, 2002). Koç Karpuz and Jansen (1992) found that the Younger Dryas off Mid Norway was colder than H1 and the Older Dryas, while Knudsen et al. (2004), Liu et al. (2012) and Oksman et al. (2017) found it was significantly warmer off Iceland and western Greenland. The diatoms of the present study show a severe cold signal at the core site during H1 as for most of the middle and late Weichselian (MIS 4–MIS 2), with extensive sea-ice cover leading to low or no phytoplankton productivity (Fig. 6a), while during at least the late part of the Younger Dryas (dissolution of diatoms in lower part) the diatom signal indicates seasonal sea-ice cover with high phytoplankton productivity, stratification and beginning influence of the Faroe Current supported by IP_{25} and biomarker data (Hoff et al., 2016) (Fig. 6a). This comparatively warm signal is in contrast to the signal from planktic foraminifera from several cores around the Faroe Islands, which showed persistent cold conditions (Rasmussen et al., 2002, 2011). Most likely the conflicting signals indicate cold subsurface water layers below a thin surface layer of warmer water during the Younger Dryas, while a thick meltwater layer with extensive sea-ice cover overlaying warmer, saline water masses existed at the Faroe Islands during H1 (see e.g., Ezat et al., 2014; Hoff et al., 2016) (Fig. 6a,c).

Andersen et al. (2004), based on diatoms found that the early Holocene had up to 4–5 °C warmer sea surface temperatures than modern, followed by a cooling trend (−4 °C) towards the later Holocene. Marine data from both the North Atlantic and the Nordic seas agree upon these basic trends with a warming of the surface waters starting ~10.5 ka and early-mid Holocene Climatic Optimum conditions between ~10 and 5 ka (e.g., Koç Karpuz and Schrader, 1990; Koç Karpuz and Jansen, 1992; Knudsen et al., 2004; Andersen et al., 2004; Berner et al., 2011). In core JM11-FI-19PC the diatoms indicate warm conditions from ~11–5 ka (Figs. 5, 6a). In the Norwegian Sea, the absolute temperature maximum occurred at 8.9–7.3 ka (Berner et al., 2011), while north of Iceland, maximum temperatures and peak relative abundance of *Sh. oestrupii* occurred at 8.8–5.5 ka (Knudsen et al., 2004). Peak percentages of *Sh. oestrupii* in our record is at ~8 ka (Fig. 5), in full agreement with previous results from the Nordic seas.

6.3. Comparison of diatoms and foraminifera: Implications

Planktic foraminiferal faunas in nearby and near-identical core ENAM93–21/MD95–2009 north of the Faroe Islands showed cold conditions in the early Eemian indicating that the Polar Front was situated south of the islands (Rasmussen et al., 1999, 2003b). However, the diatom flora shows that the surface water conditions indeed were warm, instead pointing to a much steeper, and shallower thermocline than at present north of the Faroe Islands and inflow of Atlantic surface water (Figs. 2, 5, 6a,c). These differences in temperature signals related to habitat depths of phytoplankton and foraminifera have been explored earlier in a Holocene record by Andersson et al. (2010), who came to a similar conclusion. Furthermore, based on the foraminiferal proxies from core ENAM93–21/MD95–2009 and from a core south of the Faroe Islands, Rasmussen et al. (2003b) found that the Eemian north of the Faroe Islands cooled abruptly at the boundary between MIS

5e–d. The diatoms however, indicate a much slower and gradual cooling phase that continued to the base of MIS 5c more similar to the gradual cooling seen at lower latitudes (Capron et al., 2014) (Figs. 5, 6a,c). This discrepancy between the foraminiferal and diatom data indicates that the thermocline had shallowed and become steeper similar to the early Eemian. For MIS 5d–5a (Early Weichselian), proxy temperature data of planktic foraminifera and stable isotopes from previous studies of the Nordic seas demonstrate a rather uniform cold sea surface below ~5 °C (e.g., Kellogg et al., 1978; Belanger, 1982; Fronval and Jansen, 1997; Fronval et al., 1998; Rasmussen et al., 1999). The diatoms indicated colder surface conditions and a stronger influence of the EGC/EIC, but also inflow of the warm Faroe Current and warmer surface conditions during the interstadials IS24, IS23 and IS21 (Fig. 6a). The thermocline was probably as for early and late Eemian shallower than today, but the inflow of cooler Atlantic water must have been fairly strong to sustain the high diatom and foraminiferal productivity (Fig. 6a,c). Altogether, the diatom evidence of a longer time period with Atlantic inflow during MIS 5d–5a supports previous evidence based on stable isotopes, concentrations of foraminifera and coccoliths, and species compositions of benthic foraminiferal faunas, that indicated strong convection during the warm interstadial periods (e.g., Kellogg et al., 1978; Belanger, 1982; Haake and Pflaumann, 1989; Fronval et al., 1998; Rasmussen et al., 1999).

For the Holocene, the planktic foraminifera indicate a temperature maximum beginning abruptly at ~11.2 ka (Fig. 7), which together with the diatoms indicate the establishment of a deep thermocline and strong inflow of Atlantic water. The diatoms showed that warming began ~800 years earlier with a shallow thermocline. Different microfossil proxies in MD95-2011 from the Vøring Plateau show main warming at ~11.5–11.3 ka, with surface-dwelling diatoms and coccospheres showing colder surface conditions for the first ~2000 years (Birks and Koç, 2002; Calvo et al., 2002; Dolven et al., 2002). Planktic foraminifera are thought to better reflect the flow and heat advection of Atlantic water into the Nordic seas than the shallow-dwelling flora of diatoms and coccospheres that mainly reflect orbitally controlled insolation changes in the surface mixed layer (e.g., Risebrobakken et al., 2011 and references therein). Rasmussen et al. (2014) compared Holocene benthic and planktic foraminiferal temperature signals in Atlantic water from shelf and slope areas in the northern Nordic seas and suggested that the different timings of rising temperatures and temperature maxima at the surface and subsurface were related to influence of meltwater flows in the upper water column rather than insolation. Here, we can show that the record of warm water diatom species shows only weak correlation to the insolation signal from 65°N over a time span of ~130,000 years (Fig. 6b). We also note that the records of warm water planktic foraminifera do not reflect the patterns of insolation changes (Fig. 6c). The productivity data (% TOC and to some extent the concentrations of diatoms and planktic foraminifera and $\delta^{13}C_{org}$) show stronger correlation to the orbital (and suborbital) signals (Fig. 6a,b,c).

The diatom species indicate more persistent influence of Atlantic water at the surface than the deeper-dwelling planktic foraminifera in MIS 5 and the Holocene. In MIS 4–2, the productivity of diatoms was extremely low due to extensive sea-ice cover, while the planktic foraminifera, probably due to their subsurface habitat and less dependence on sun light, were more resilient.

7. Conclusions

Diatom data from the central north Faroe slope and multivariate analysis gave five diatom assemblage zones (DAZ1–5) representing five main oceanographic and climatic subdivisions of the last ~130,000 years.

In the glacial Marine Isotope Stage (MIS) 6/5 transition > 130 ka, cold Arctic surface water and extensive sea-ice cover, was replaced by an increasing influence of the Faroe Current bringing warm, saline

Atlantic surface water into the area. The Arctic Front retreated northward. During the penultimate interglacial the Eemian, warm surface conditions and an enhanced influence of the Faroe Current occurred at 130–113 ka (MIS 5e and lower MIS 5d). The Iceland-Faroe Front did not develop, apparently due to a weaker influence of the cold and low-saline East Greenland and East Icelandic currents. The early part of the Weichselian (113–86 ka, upper MIS 5d to 5b) shows continued influence of inflowing warm Atlantic water, but with a gradual shift to more cold Arctic water with increased influence of the East Greenland Current/East Icelandic Current and seasonal sea-ice cover. The Arctic Front was mostly close to or southeast of the core site. The middle-late Weichselian MIS 5a–2, 86–14.5 ka began with renewed inflow of warmer Atlantic surface water during MIS 5a, while MIS 4–2 showed cold conditions, with extensive sea-ice cover close to or north of the Polar Front with only small warmings during the larger and warmest interstadials. The Iceland-Faroe Front established in the area in the earliest Holocene. The Holocene from 11 ka showed warmer sea surface conditions than today, with a strong influence of the Faroe Current until 5 ka, where cooling began.

Comparison of the distribution patterns of diatoms (surface mixed layer) with planktic foraminifera (subsurface thermocline) provided a more complex picture of the changes in the structure of the upper water column. The diatoms showed an earlier, gradual and longer-lasting influence of warm Atlantic water of the Faroe Current in the surface mixed layer in the Eemian and Holocene intervals than the foraminifera and similar early warming and later gradual cooling signals in the large interstadials in MIS 5d–5a, with a steep thermocline existing in these transgressive periods. The long-lasting warm conditions and inflow of Atlantic Water confirm earlier results based on benthic proxies that have indicated strong convection for extended periods in MIS 5. Our results are a clear indication that the surface-dwelling diatoms respond primarily to changes in the surface water and the inflow of Atlantic water, degree of sea-ice cover, and first secondarily to insolation change.

References

Abbott, P.M., Austin, W.E.N., Davies, S.M., Pearce, N.J.G., Rasmussen, T.L., Wastegård, S., Brendryen, J., 2014. Re-evaluation and extension of the Marine Isotope Stage 5 tephrostratigraphy of the Faroe Islands region: the cryptotephra record. Palaeogeogr. Palaeoclimatol. Palaeoecol. 409, 153–168.

Alonso-Garcia, M., Sierro, F.J., Flores, J.A., 2011. Arctic front shifts in the subpolar North Atlantic during the Mid-Pleistocene (800–400 ka) and their implications for ocean circulation. Palaeogeogr. Palaeoclimatol. Palaeoecol. 311, 268–280.

Andersen, C., Koç, N., Jennings, A., Andrews, J.T., 2004. Nonuniform response of the major surface currents in the Nordic seas to insolation forcing: Implications for the Holocene climate variability. Paleoceanography 19, PA2003. https://doi.org/10.

1029/2002PA000873.

Andersson, C., Pausata, F.S.R., Jansen, E., Risebrobakken, B., Telford, R.J., 2010. Holocene trends in the foraminifer record from the Norwegian Sea and the North Atlantic Ocean. Clim. Past 6, 179–193.

Andrews, J.T., Giraudeau, J., 2003. Multi-proxy records showing significant Holocene environmental variability: the inner N. Iceland shelf (Hunafloi). Quat. Sci. Rev. 22, 175–193.

Balbon, E., 2000. Variabilité climatique et circulation thermohaline dans l'Ocean Atlantique nord et en Mer de Norvège au cours du Quaternaire Superieur. University of Paris, Paris, France, PhD dissertation.

Barron, J.A., 1992. Pliocene paleoclimatic interpretation of DSDP Site 580 (NW Pacific) using diatoms. Mar. Micropaleontol. 20, 23–44.

Bauch, D., Carstens, J., Wefer, G., 1997. Oxygen isotope composition of living *Neogloboquadrina pachyderma* (sin.) in the Arctic Ocean. Earth Planet. Sci. Lett. 146, 47–58.

Bauch, H.A., Erlenkeuser, H., Fahl, K., Spielhagen, R.F., Weinelt, M.S., Andruleit, H., Henrich, R., 1999. Evidence for a steeper Eemian than Holocene sea surface temperature gradient between Arctic and sub-Arctic regions. Palaeogeogr. Palaeoclimatol. Palaeoecol. 145, 95–117.

Bauch, H.A., Kandiano, E.S., Helmke, J., Andersen, N., Rosell-Mele, A., Erlenkeuser, H., 2011. Climatic bisection of the last interglacial warm period in the Polar North Atlantic. Quat. Sci. Rev. 30, 1813–1818.

Bauch, H.A., Kandiano, E.S., Helmke, J.P., 2012. Contrasting ocean changes between the subpolar and polar North Atlantic during the past 135 ka. Geophys. Res. Lett. 39 (L11604), 1–7.

Bé, A.W.H., Tolderlund, D.S., 1971. Distribution and ecology of living planktonic foraminifera in surface waters of the Atlantic and Indian Oceans. In: Funnel, B.M., Riedel, W.R. (Eds.), The Micropaleontology of the Oceans. Cambridge University Press, London, pp. 105–149.

Belanger, P.E., 1982. Paleo-oceanography of the Norwegian Sea during the past 130,000 years: coccolithophorid and foraminiferal data. Boreas 11, 29–36.

Belt, S.T., Müller, J., 2013. The Arctic sea-ice biomarker IP25: a review of current understanding, recommendations for future research and applications in palaeo sea-ice reconstructions. Quat. Sci. Rev. 79, 9–25.

Berger, A., Loutre, M.F., 1991. Insolation values for the climate of the last 10 million years. Quat. Sci. Rev. 10, 297–317.

Berner, K.S., Koc, N., Divine, D., Godtliebsen, F., Moros, M., 2008. A decadal-scale Holocene sea surface temperature record from the subpolar North Atlantic constructed using diatoms and statistics and its relation to other climate parameters. Paleoceanography 23, PA2210. https://doi.org/10.1029/2006PA001339.

Berner, K.S., Koc, N., Godtliebsen, F., Divine, D., 2011. Holocene climate variability of the Norwegian Atlantic Current during high and low solar insolation forcing. Paleoceanography 26, PA2220. https://doi.org/10.1029/2012PA002002.

Birks, C.J.A., Koç, N., 2002. A high-resolution record of late-Quaternary sea-surface temperatures and oceanographic conditions from the eastern Norwegian Sea. Boreas 31, 323–344.

Bond, G., Broecker, W., Johnsen, S., McManus, J., Labeyrie, L., Jouzel, J., Bonani, G., 1993. Correlations between climate records from North Atlantic sediments and Greenland ice. Nature 365, 143–147.

Born, A., Nisancioglu, K., Braconnot, P., 2010. Sea ice induced changes in ocean circulation during the Eemian. Clim. Dyn. 35, 1361–1371.

Broecker, W.S., 1991. The great ocean conveyor. Oceanography 4, 79–89.

Broecker, W.S., Denton, G.H., 1989. The role of ocean-atmosphere reorganizations in glacial cycles. Geochim. Cosmochim. Acta 53, 2465–2501.

Calvert, S.E., Pedersen, T.F., 1992. Organic carbon accumulation and preservation in marine sediments: how important is anoxia? In: Whelan, J.K., Farrington, J.W. (Eds.), Productivity, Accumulation and Preservation of Organic Matter in Recent and Ancient Sediments. Columbia University Press, Columbia, pp. 231–263.

Calvo, E., Grimalt, J., Jansen, E., 2002. High resolution U^k_{37} sea surface temperature reconstruction in the Norwegian Sea during the Holocene. Quat. Sci. Rev. 21, 1385–1394.

Canfield, D.E., 1994. Factors influencing organic carbon preservation in marine sediments. Chem. Geol. 114, 315–329.

Capron, E., Govin, A., Stone, E.J., Masson-Delmotte, V., Mulitza, S., Otto-Bliesner, B., Rasmussen, T.L., Sime, L.C., Waelbroeck, C., Wolff, E.W., 2014. Temporal and spatial structure of multi-millennial temperature changes at high latitudes during the Last Interglacial. Quat. Sci. Rev. 103, 116–133.

Carstens, J., Wefer, G., 1992. Recent distribution of planktonic foraminifera in the Nansen Basin, Arctic Ocean. Deep-Sea Res. 39, 507–524.

Cortijo, E., Duplessy, J.C., Labeyrie, L., Leclaire, H., Duprat, J., van Wearing, T.C.E., 1994. Eemian cooling in the Norwegian Sea and North Atlantic Ocean preceding continental ice-sheet growth. Nature 372, 446–449.

Crosta, X., Pichon, J.-J., Labracherie, M., 1997. Distribution of *Chaetoceros* resting spores in modern peri-Antarctic sediments. Mar. Micropaleontol. 29, 283–299.

Crucifix, M., Loutre, F., 2002. Transient simulations over the last interglacial period (126–115 kyr BP): feedback and forcing analysis. Clim. Dyn. 19, 417–433.

Dansgaard, W., Johnsen, S.J., Clausen, H.B., Dahl-Jensen, D., Gundestrup, N.S., Hammer, C.U., Hvidberg, C.S., Steffensen, J.P., Sveinbjørnsdottir, A.E., Jouzel, J., Bond, G., 1993. Evidence for general instability of past climate from a 250-kyr ice-core record. Nature 364, 218–220.

Darling, K.F., Kucera, M., Kroon, D., Wade, C.M., 2006. A resolution for the coiling direction paradox in *Neogloboquadrina pachyderma*. Paleoceanography 21https://doi.org/10.1029/2005PA001189. PA2011.

Davies, S.M., Wastegård, S., Rasmussen, T.L., Johnsen, S.J., Steffensen, J.P., Andersen, K.K., Svensson, A., 2008. Identification of the Fugloyarbanki Tephra in the NGRIP ice-core: a key tie-point for marine and ice-core sequences during the last glacial

period. Journal of Quaternary Science, Rapid Communication 23, 409–414.

Davies, S.M., Wastegård, S., Abbott, P.M., Barbante, C., Bigler, M., Johnsen, S.J., Rasmussen, T.L., Steffensen, J.P., Svensson, A., 2010. Tracing volcanic events in the NGRIP ice-core and synchronising North Atlantic marine records during the last glacial period. Earth Planet. Sci. Lett. 294, 69–79.

Davies, S.M., Abbott, P.M., Meara, R.H., Pearce, N.J.G., Austin, W.E.N., Chapman, M.R., Svensson, A., Bigler, M., Rasmussen, T.L., Rasmussen, S.O., Farmer, E.J., 2014. A North Atlantic tephrostratigraphical framework for 130–60 ka b2k: new tephra discoveries, marine-based correlations, and future challenges. Quat. Sci. Rev. 106, 101–121.

Deser, C., Teng, H., 2008. Evolution of Arctic sea-ice concentration trends and the role of atmospheric circulation forcing, 1979–2007. Geophys. Res. Lett. 35, L02504.

Dolven, J.K., Cortese, G., Bjørklund, K.R., 2002. A high-resolution radiolarian-derived palaeotemperature record for the Late Pleistocene-Holocene in the Norwegian Sea. Paleoceanography 17, 1072. https://doi.org/10.1029/2002PA000780.

Dooley, H.D., Meincke, J., 1981. Circulation and water masses in the Faeroese Channels during Overflow '73. Deutsche Hydrographische Zeitschrift 34, 41–55.

Emerson, S., Hedges, J.I., 1988. Processes controlling the organic carbon content of open ocean sediments. Paleoceanography 3, 621–634.

Ezat, M.M., Rasmussen, T.L., Groeneveld, J., 2014. Persistent intermediate water warming during cold stadials in the southeastern Nordic seas during the past 65 k.y. Geology 42, 663–666.

Ezat, M.M., Rasmussen, T.L., Groeneveld, J., 2016. Reconstruction of hydrographic changes in the southern Norwegian Sea during the past 135 kyr and the impact of different foraminiferal Mg/Ca cleaning protocols. Geochem. Geophys. Geosyst. 17, 3420–3436.

Fronval, T., Jansen, E., 1996. Rapid changes in ocean circulation and heat flux in the Nordic Seas during the last Interglacial period. Nature 383, 806–810.

Fronval, T., Jansen, E., 1997. Eemian and early Weichselian (140–60 ka) paleoceanography and paleoclimate in the Nordic seas with comparisons to Holocene conditions. Paleoceanography 12, 443–462.

Fronval, T., Jansen, E., Haflidason, H., Sejrup, H.P., 1998. Variability in surface and deep water conditions in the Nordic seas during the last interglacial period. Quat. Sci. Rev. 17, 963–985.

Fryxell, G.A., Hasle, G.R., 1972. *Thalassiosira eccentrica* (Ehrenb.) Cleve, *T. symmetrica* sp. nov., and some related centric diatoms. J. Phycol. 8, 297–317.

Fryxell, G.A., Hasle, G.R., 1980. The marine diatom *Thalassiosira oestrupii*: structure, taxonomy and distribution. Am. J. Bot. 67, 804–814.

Gersonde, R., Zielinski, U., 2000. The reconstruction of late Quaternary Antarctic sea-ice distribution — the use of diatoms as a proxy for sea-ice. Palaeogeogr. Palaeoclimatol. Palaeoecol. 162, 263–286.

Grimm, E.C., 1991. Tilia 1.12, Tilia-Graph 1.18. Illinois State Museum, Research and Collection Center, Springfield.

Haake, F.-W., Pflaumann, U., 1989. Late Pleistocene stratigraphy on the Vøring Plateau, Norwegian Sea. Boreas 18, 343–356.

Hansen, B., Østerhus, S., 2000. North Atlantic-Nordic seas exchanges. Prog. Oceanogr. 45, 109–208.

Hansen, B., Østerhus, S., Dooley, H.D., Gould, W.J., Rickards, L.J., 1998. North Atlantic-Norwegian Sea Exchanges: the ICES NANSEN Project. ICES Cooperative Research Reports 255, 948.

Hasle, G.R., 1978. Some *Thalassiosira* species with one central process (Bacillariophyceae). Nor. J. Bot. 25, 77–110.

Hasle, G.R., Fryxell, G.A., 1977. The genus *Thalassiosira*: some species with a linear areola array. Nova Hedwigia 54, 15–66.

Hasle, G.R., Syvertsen, E.E., 1997. Marine Diatoms. In: Tomas, C.R. (Ed.), Identifying Marine Phytoplankton. Academic Press Inc., San Diego, pp. 5–385.

Hebbeln, D., Henrich, R., Baumann, K.H., 1998. Paleoceanography of the last interglacial/glacial cycle in the polar North Atlantic. Quat. Sci. Rev. 17, 125–153.

Heinrich, H., 1988. Origin and consequences of cyclic ice rafting in the Northeast Atlantic Ocean during the past 130,000 years. Quat. Res. 29, 142–152.

Hemleben, C., Spindler, M., Anderson, O.R., 1989. Modern Planktonic Foraminifera. Springer-Verlag, New York, pp. 363.

Hoff, U., Rasmussen, T.L., Stein, R., Ezat, M.M., Fahl, K., 2016. Sea ice and millennial-scale climate variability in the Nordic seas 90 kyr ago to present. Nat. Commun. 7. https://doi.org/10.1038/ncomms12247.

Hopkins, T.S., 1991. The GIN-Sea — a synthesis of its physical oceanography and literature review 1972–1985. Earth Sci. Rev. 30, 175–318.

Horner, R.A., 1982. Do ice algae produce the spring phytoplankton bloom in seasonally ice-covered waters? In: Mann, D.G. (Ed.), Seventh Diatom Symposium. Otto Koeltz Science Publishers, London, pp. 401–409.

Horner, R.A. (Ed.), 1985. Sea Ice Biota. CRC Press, Boca Raton, Florida, pp. 215.

Hustedt, F., 1930. Die Kieselalgen Deutschlands, Österreichs und der Schweiz unter Berücksichtigung der übrigen Länder Europas, sowie der angrenzenden Meeresgebiete. In: Rabenhorst, L. (Ed.), Kryprogamenflora von Deutschland, Österreich und der Schweiz, Teil 1. Akademische Verlagsgesellschaft, Leipzig, pp. 920 (in German).

Hustedt, F., 1959. Die Kieselalgen Deutschlands, Österreichs und der Schweiz unter Berücksichtigung der übrigen Länder Europas, sowie der angrenzenden Meeresgebiete. In: Rabenhorst, L. (Ed.), Kryprogamenflora von Deutschland, Österreich und der Schweiz, Teil 2. Akademische Verlagsgesellschaft, Leipzig, pp. 845 (in German).

Jansen, E., Bjørklund, K., 1985. Surface ocean circulation in the Norwegian Sea 15,000 B.P. to present. Boreas 14, 243–257.

Jiang, H., 1996. Diatoms from the surface sediments of the Skagerrak and the Kattegat and their relationship to the spatial changes of environmental variables. J. Biogeogr. 23, 129–137.

Jiang, H., Seidenkrantz, M.S., Knudsen, K.L., Eiríksson, J., 2001. Diatom surface sediment assemblages around Iceland and their relationships to oceanic environmental variables. Mar. Micropaleontol. 41, 73–96.

Jiang, H., Seidenkrantz, M.S., Knudsen, K.L., Eiríksson, J., 2002. Late-Holocene summer sea-surface temperatures based on a diatom record from the north Icelandic shelf. The Holocene 12, 137–147.

Jiang, H., Muscheler, R., Björck, S., Seidenkrantz, M.-S., Olsen, J., Sha, L., Sjolte, J., Eiriksson, J., Ran, L., Knudsen, K.-L., Knudsen, M.F., 2015. Solar forcing of Holocene summer sea-surface temperatures in the northern North Atlantic. Geology 43, 203–206.

Jousé, A.P., Kozlova, O.G., Mukhina, V.V., 1971. Distribution of diatoms in the surface layer of sediment from the Pacific Ocean. In: Funnel, B.M., Riedel, W.R. (Eds.), Micropaleontology of Oceans. Cambridge University Press, Cambridge, pp. 263–269.

Jouzel, J., Vimeux, F., Caillon, N., Delaygue, G., Hoffmann, G., Masson-Delmotte, V., Parrenin, F., 2003. Magnitude of isotope/temperature scaling for interpretation of central Antarctic ice cores. J. Geophys. Res. 108, 4361. https://doi.org/10.1029/2002JD002677.

Juggins, S., 1992. Diatoms in the Thames Estuary, England: ecology, paleoecology, and salinity transfer function. Bibliotheca Diatomologica, Vol. 25. J. Cramer, Stuttgart, Germany, pp. 1–216.

Justwan, A., Koç, N., 2008. A diatom based transfer function for reconstructing sea ice concentrations in the North Atlantic. Mar. Micropaleontol. 66, 264–278.

Kanaya, T., Koizumi, I., 1966. Interpretation of diatom thanatocoenosis from the North Pacific applied to a study of core V 20-130. Tohoku University, Scientific Reports, Series 2, 89–130.

Kellogg, T.B., Duplessy, J.C., Shackleton, N.J., 1978. Planktonic foraminiferal and oxygen isotopic stratigraphy and paleoclimatology of Norwegian Sea deep-sea cores. Boreas 7, 61–73.

Knudsen, K.L., Jiang, H., Jansen, E., Eiríksson, J., Heinemeier, J., Seidenkrantz, M.S., 2004. Environmental changes off North Iceland during the deglaciation and the Holocene: foraminifera, diatoms and stable isotopes. Mar. Micropaleontol. 50, 273–305.

Koç Karpuz, N., 1989. Surface Sediment Distribution and Holocene Paleotemperature Variations in the GIN Sea. Cand. Scient. Thesis. University of Bergen, Norway, pp. 199.

Koç Karpuz, N., Jansen, E., 1992. A high-resolution diatom record of the last deglaciation from the SE Norwegian Sea: documentation of rapid climatic changes. Paleoceanography 7, 499–520.

Koç Karpuz, N., Schrader, H., 1990. Surface sediment diatom distribution and Holocene paleotemperature variations in the Greenland, Iceland and Norwegian seas. Paleoceanography 5, 557–580.

Koç, N., Jansen, E., Haflidason, H., 1993. Paleoceanographic reconstructions of surface ocean conditions in the Greenland, Iceland and Norwegian seas through the last 14 ka based on diatoms. Quat. Sci. Rev. 12, 115–140.

Kohly, A., 1998. Diatom flux and species composition in the Greenland Sea and the Norwegian Sea in 1991-1992. Mar. Geol. 145, 293–312.

Krawczyk, D., Witkowski, A., Moros, M., Lloyd, J., Kuijpers, A., Kierzek, A., 2010. Late-Holocene diatom inferred reconstruction of temperature variations of the West Greenland Current from Disko Bugt, central West Greenland. The Holocene 20, 659–666.

Krawczyk, D.W., Witkowski, A., Wroniecki, M., Waniek, J., Kurzydłowski, K.J., Płociński, T., 2012. Reinterpretation of two diatom species from the West Greenland margin – *Thalassiosira kushirensis* and *Thalassiosira antarctica* var. *borealis* – hydrological consequences. Mar. Micropaleontol. 88–89, 1–14.

Krawczyk, D., Witkowski, A., Moros, M., Lloyd, J., Høyer, J.L., Miettinen, A., Kuijpers, A., 2017. Quantitative reconstruction of Holocene sea ice and sea surface temperature off West Greenland from the first regional diatom set. Paleocenography 32, 18–40.

Labeyrie, L.D., Duplessy, J.-C., 1985. Changes in oceanic $^{13}C/^{12}C$ ratio during the last 140,000 years: high-latitude surface water records. Palaeogeogr. Palaeoclimatol. Palaeoecol. 50, 217–240.

Lisiecki, L.E., Raymo, M.E., 2005. A Pliocene-Pleistocene stack of 57 globally distributed benthic $\delta^{18}O$ records. Paleoceanography 20. https://doi.org/10.1029/2004PA0010171.

Liu, Z., Carlson, A.E., He, F., Brady, E.C., Otto-Bliesner, B.L., Briegleb, B.P., Wehrenberg, M., Clark, P.U., Wu, S., Cheng, J., Zhang, J., Noone, D., Zhu, J., 2012. Younger Dryas cooling and the Greenland climate response to CO_2. PNAS 109, 11,101–11,104.

Malmberg, S.A., 1985. The water masses between Iceland and Greenland. J. Mar. Res. 9, 127–140.

Maynard, N.G., 1976. Relationship between diatoms in surface sediments of the Atlantic Ocean and the biological and physical oceanography of overlying waters. Paleobiology 2, 99–121.

Matul, A., Spielhagen, R.F., Kazarina, G., Kruglikova, S., Dmitrenko, O., Mohan, R., 2018. Warm-water events in the eastern Fram Strait during the last 2000 years as revealed by different microfossil groups. Polar Res. 37. https://doi.org/10.1080/17518369.2018.1540243.

McManus, J.F., Oppo, D.W., Keigwin, L.D., Cullen, J.L., Bond, G.C., 2002. Thermohaline circulation and prolonged interglacial warmth in the North Atlantic. Quat. Res. 58, 17–21.

Meyers, P.A., 1994. Preservation of elemental and isotopic source identification of sedimentary organic material. Chem. Geol. 114, 289–302.

Meyers, P.A., 1997. Organic geochemical proxies of paleoceanographic, paleolimnologic, and paleoclimatic processes. Org. Geochem. 27, 213–250.

Meyers, P.A., 2003. Applications of organic geochemistry to palaeolimnological reconstructions: a summary of examples from the Laurentian Great Lakes. Org. Geochem. 34, 261–289.

Miettinen, A., Divine, D., Koç, N., Godtliebsen, F., Hall, I.R., 2012. Multicentennial variability of the sea surface temperature gradient across the Subpolar North Atlantic over the last 2.8 kyr. J. Clim. 25, 4205–4219.

Miettinen, A., Koç, N., Hall, I.R., Godtliebsen, F., Divine, D., 2011. North Atlantic sea surface temperatures and their relation to the North Atlantic Oscillation during the last 230 years. Clim. Dyn. 36, 533–543.

Miettinen, A., Divine, D., Husum, K., Koç, N., Jennings, A., 2015. Exceptional ocean surface conditions on the SE Greenland shelf during the Medieval Climate Anomaly. Paleoceanography 30, 1657–1674.

Moros, M., Emeis, K., Risebrobakken, B., Snowball, I., Kuijpers, A., McManus, J., Jansen, E., 2004. Sea surface temperatures and ice rafting in the Holocene North Atlantic: climate influences on northern Europe and Greenland. Quat. Sci. Rev. 23, 2113–2126.

Mukhina, V.V., Dmitrenko, O.B., 2008. Microfossils in the Upper Quaternary sediments of the Norwegian Sea (biostratigraphy and paleoceanology). Mar. Geol. 48, 720–734.

Müller, J., Stein, R., 2014. High-resolution record of late glacial and deglacial sea ice changes in Fram Strait corroborates ice-ocean interactions during abrupt climate shifts. Earth Planet. Sci. Lett. 403, 446–455.

Müller, J., Massé, G., Stein, R., Belt, S.T., 2009. Variability of sea-ice conditions in the Fram Strait over the past 30,000 years. Nat. Geosci. 2, 772–776.

Oksman, M., Weckström, K., Miettinen, A., Juggins, S., Divine, D.V., Jackson, R., Telford, R., Korsgaard, N.J., Kucera, M., 2017. Younger Dryas ice margin retreat triggered by ocean surface warming in central-eastern Baffin Bay. Nature Communications 18. https://doi.org/10.1038/s41467-017-01155-6.

Oksman, M., Juggins, S., Miettinen, A., Witkowski, A., Weckström, K., 2019. The biogeography and ecology of common diatom species in the northern North Atlantic, and their implications for paleoceanographic reconstructions. Mar. Micropaleontol. 148. https://doi.org/10.1016/j.marmicro.2019.02.002.

Orme, L.C., Miettinen, A., Divine, D., Husum, K., Pearce, C., van Nieuwenhove, N., Born, A., Mohan, R., Seidenkrantz, M.-S., 2018. Subpolar North Atlantic sea surface temperature since 6 ka BP: indications of anomalous ocean-atmosphere interactions at 4–2 ka BP. Quat. Sci. Rev. 194, 128–142.

Orvik, K.A., Niiler, P., 2002. Major pathways of Atlantic water in the northern North Atlantic and Nordic Seas toward Arctic. Geophys. Res. Lett. 29. https://doi.org/10.1029/2002GL015002.

Pearce, C., Seidenkrantz, M.-S., Kuijpers, A., Reynisson, N.F., 2014. A multi-proxy reconstruction of oceanographic conditions around the Younger Dryas-Holocene transition in Placentia Bay, Newfoundland. Mar. Micropaleontol. 112, 39–49.

Railsback, L.B., Gibbard, P.L., Head, M.J., Voarintsoa, N.R.G., Toucanne, S., 2015. An optimized scheme of lettered marine isotope substages for the last 1.0 million years, and the climatostratigraphic nature of isotope stages and substages. Quat. Sci. Rev. 111, 94–106.

Ramsfjell, E., 1960. Phytoplankton distribution in the Norwegian Sea in June, 1952 and 1953. Fiskeridirektoratets Skrifter serie Havundersøkelser 12, 1–40.

Ran, L., Jiang, H., Knudsen, K.L., Eiriksson, J., 2008. A high-resolution Holocene diatom record on the North Icelandic shelf. Boreas 37, 399–413.

Rasmussen, T.L., Thomsen, E., 2004. The role of the North Atlantic Drift in the millennial timescale glacial climate fluctuations. Palaeogeogr. Palaeoclimatol. Palaeoecol. 210, 101–116.

Rasmussen, T.L., Thomsen, E., Labeyrie, L., van Weering, T.C.E., 1996a. Circulation changes in the Faeroe-Shetland Channel correlating with cold events during the last glacial period (58–10 ka). Geology 24, 937–940.

Rasmussen, T.L., van Weering, T.C.E., Labeyrie, L., 1996b. High resolution stratigraphy of the Faeroe-Shetland Channel and its relation to North Atlantic paleoceanography: the last 87 ka. Mar. Geol. 131, 75–88.

Rasmussen, T.L., Thomsen, E., van Weering, T.C.E., Labeyrie, L., 1996c. Rapid changes in surface and deep water conditions at the Faeroe Margin during the last 58,000 years. Paleoceanography 11, 757–771.

Rasmussen, T.L., Balbon, E., Thomsen, E., Labeyrie, L., van Weering, T.C.E., 1999. Climate records and changes in deep outflow from the Norwegian Sea ~150–55 ka. Terra Nova 11, 61–66.

Rasmussen, T.L., Bäckström, D., Heinemeier, J., Klitgaard-Kristensen, D., Knutz, P.C., Kuijpers, A., Lassen, S., Thomsen, E., Troelstra, S.R., van Weering, T.C.E., 2002. The Faeroe-Shetland Gateway: Late Quaternary water mass exchange between the Nordic seas and the northeastern Atlantic. Mar. Geol. 188, 165–192.

Rasmussen, T.L., Wastegård, S., Kuijpers, A., van Weering, T.C.E., Heinemeier, J., Thomsen, E., 2003a. Stratigraphy and distribution of tephra layers in marine sediment cores from the Faeroe Islands, North Atlantic. Mar. Geol. 199, 263–277.

Rasmussen, T.L., Thomsen, E., Kuijpers, A., Wastegård, S., 2003b. Late warming and early cooling of the sea surface in the Nordic seas during MIS 5e (Eemian Interglacial). Quat. Sci. Rev. 22, 809–821.

Rasmussen, T.L., Thomsen, E., Nielsen, T., Wastegård, S., 2011. Atlantic surface Water inflow to the Nordic seas during the Pleistocene-Holocene transition (mid Younger Dryas to Pre-Boreal periods, 12,450–10,000 cal years BP). J. Quat. Sci. 26, 723–733.

Reigstad, M., Carroll, J., Slagstad, D., Ellingsen, I., Wassmann, P., 2011. Intra-regional comparison of productivity, carbon flux and ecosystem composition within the northern Barents Sea. Prog. Oceanogr. 90, 33–46.

Reimer, P.J., Bard, E., Beck, J.W., Baillie, M.G.L., Blackwell, P.G., Bronk Ramsey, C., Buck, C.E., Cheng, H., Edwards, R.L., Friedrich, M., Grootes, P.M., Guilderson, T.P., Haflidason, H., Hajdas, I., Hatte, M., Heaton, T.J., Hoffmann, D.L., Hogg, A.G., Hughen, K.A., Kaiser, K.F., Kromer, B., Manning, S.W., Niu, M., Reimer, R.W., Richards, D.A., Scott, E.M., Southon, J.R., Staff, R.A., Turney, C.S.M., van der Plicht, J., 2013. IntCal13 and Marine13 radiocarbon age calibration curves, 0–50,000 years cal BP. Radiocarbon 55, 1869–1887.

Rasmussen, T.L., Thomsen, E., Nielsen, T., 2014. Water mass exchange between the Nordic seas and the Arctic Ocean on millennial time scale during MIS 4-MIS 2. Geochem. Geophys. Geosyst. 15, 530–544. https://doi.org/10.1002/2013GC005020.

Risebrobakken, B., Jansen, E., Andersson, C., Mjelde, E., Hevrøy, K., 2003. A high-

resolution study of Holocene paleoclimate and paleoceanographic changes in the Nordic Seas. Paleoceanography 18, 1017–1031.

Risebrobakken, B., Dokken, T., Smedsrud, L.H., Andersson, C., Jansen, E., Moros, M., Ivanova, E.V., 2011. Early Holocene temperature variability in the Nordic Seas: the role of ocean heat advection versus changes in orbital forcing. Paleoceanography 26, PA4206. https://doi.org/10.1029/2011PA002117.

Sancetta, C., 1982. Distribution of diatom species in surface sediments of the Bering and Okhotsk seas. Micropaleontology 28, 221–257.

Sanchez-Goñi, M.F., Harrison, S.P., 2010. Millennial-scale climate variability and vegetation changes during the Last Glacial: Concepts and terminology. Quat. Sci. Rev. 29, 2823–2827.

Schrader, H., Gersonde, R., 1978. Diatoms and silicoflagellates. Utrecht Micropaleontol. Bull. 17, 129–176.

Schrader, H., Lindström-Swanberg, I., Burckle, L.H., Grønlien, L., 1993a. Diatoms in recent Atlantic (20°S to 70°N latitude) sediments: abundance patterns and what they mean. Hydrobiologia 269 (270), 129–135.

Schrader, H., Isrenn, K., Swanberg, N., Paetzel, M., Seathre, T., 1993b. Early Holocene diatom pulse in the Norwegian Sea and its paleoceanographic significance. Diatom Research 8, 117–130.

Sha, L., Jiang, H., Knudsen, K.L., 2011. Diatom evidence of climatic change in Holsteinborg Dyb, west of Greenland, during the last 1200 years. The Holocene 22, 347–358.

Shackleton, N.J., Opdyke, N.D., 1973. Oxygen isotope and paleomagnetic stratigraphy of Equatorial Pacific core V28-238; oxygen isotope temperature and ice volumes on a 10^5 year to 10^6 year scale. Quat. Res. 3, 39–55.

Simonsen, R., 1974. The diatom plankton of the Indian Ocean Expedition of R. V. *Meteor* 1964-1965. *Meteor* Forschungsergebnisse. Reihe D 19, 1–66.

Ślubowska-Woldengen, M., Rasmussen, T.L., Koç, N., Klitgaard-Kristensen, D., Nilsen, F., Solheim, A., 2007. Advection of Atlantic Water to the western and northern Svalbard shelf since 17,500 cal yr BP. Quat. Sci. Rev. 26, 463–478.

Smayda, T.J., 1969. Experimental observations on the influence of temperature, light, and salinity on cell division of the marine diatom *Detonula confervacea* (Cleve) Gran2. J. Phycol. 5, 150–157.

Smith, S.L, Smith, W.O., Codispodi, L.A., Wilson, D.L., 1985. Biological observations in the marginal ice zone of the East Greenland Sea. J. Mar. Res. 43, 693–717.

Søgaard, H., 1996. Climate and weather. In: Guttesen, R. (Ed.), Atlas of Denmark Series II. The Færoe Islands Topographical Atlas, vol. 5. Ca.A. Reitzels Forlag for Det Kongelige Danske Selskab og Kort og Matrikelstyrelse, Copenhagen, pp. 24–27.

Streeter, S.S., Belanger, P.E., Kellogg, T.B., Duplessy, J.-C., 1982. Late Pleistocene paleoceanography of the Norwegian-Greenland Sea: benthic foraminiferal evidence. Quat. Res. 18, 72–90.

Sundström, B.G., 1986. The marine diatom genus *Rhizosolenia*. Ph.D. thesis. University of Lund, Sweden, pp. 117, 39 pl.

Svensson, A., Andersen, K.K., Bigler, M., Clausen, H.B., Dahl-Jansen, D., Davies, S.M., Johnsen, S.J., Muscheler, R., Parrenin, F., Rasmussen, S.O., Röthlisberger, R., Seierstad, I., Steffensen, J.P., Vinther, B.M., 2008. A 60 000 year Greenland

stratigraphic ice core chronology. Clim. Past 4, 47–57.

Swift, J.H., 1986. The Arctic waters. In: Hurdle, B.G. (Ed.), The Nordic Seas. Springer–Verlag, New York, pp. 124–153.

Syvertsen, E.E., 1979. Resting spore formation in clonal cultures of *Thalassiosira antarctica* Comber, *Ts. nordenskioldii* Cleve and *Detonula confervacea* (Cleve) Gran. Nova Hedwigia 64, 41–63.

Tzedakis, P.C., 2005. Towards an understanding of the response of southern European vegetation to orbital and suborbital climate variability. Quat. Sci. Rev. 24, 1585–1599.

Van Aken, H.M., 1988. Transports of water masses through the Faroese Channels determined by an inverse method. Deep-Sea Res. 35, 595–617.

Wastegård, S., Rasmussen, T.L., 2001. New tephra horizons from oxygen isotope stage 5 in the North Atlantic: correlation potential for terrestrial, marine and ice-core archives. Quat. Sci. Rev. 20, 1587–1593.

Wastegård, S., Rasmussen, T.L., 2014. Faroe Marine Ash Zone IV — a new MIS3 ash zone on the Faroe Islands margin. Geol. Soc. Spec. Publ. 398, 81–93.

Wastegård, S., Rasmussen, T.L., Kuijpers, A., Nielsen, T., van Weering, T.C.E., 2006. Composition and origin of ash zones from Marine Isotope Stages 3 and 2 in the North Atlantic. Quat. Sci. Rev. 25, 2409–2419.

Weckström, K., Miettinen, A., Caissie, B., Pearce, C., Ellegaard, M., Krawczyk, D., Witkowski, A., 2014. Sea surface temperatures in Disko Bay during the Little Ice Age – caution needs to be exercised before assigning *Thallasiosira kushirensis* resting spore as a warm-water indicator in palaeoceanographic studies. Quat. Sci. Rev. 101, 234–237.

Williams, K.M., 1986. Recent Arctic marine diatom assemblages from bottom sediments in Baffin Bay and Davies Strait. Mar. Micropaleontol. 10, 327–341.

Witak, M., Wachnicka, A., Kuijpers, A., Troelstra, S., Prins, M.A., Witkowski, A., 2005. Holocene North Atlantic surface circulation and climate variability: evidence from diatom records. The Holocene 15, 85–96.

Witkowski, A., Lange-Bertalot, H., Metzeltin, D., 2000. Diatom flora of marine coasts: I. In: Lange-Bertalot, H. (Ed.), Iconographia Diatomologica. Volume 7. A.R.G, Gantner, Germany, pp. 905.

Witon, E., Malmgren, B., Witkowski, A., Kuijpers, A., 2006. Holocene marine diatoms from the Faeroe Islands and their paleoceanographic implications. Palaeogeogr. Palaeoclimatol. Palaeoecol. 239, 487–509.

Wolff, E.W., Chappellaz, J., Blunier, T., Rasmussen, S.O., Svensson, A., 2010. Millennial-scale variability during the last glacial: the ice core record. Quat. Sci. Rev. 29, 2828–2838.

Zamelczyk, K., Rasmussen, T.L., Husum, K., Haflidason, H., de Vernal, A., Ravna, E.K., Hald, M., Hillaire-Marcel, C., 2012. Between two oceanic fronts: paleoceanographic changes and calcium carbonate dissolution in the central Fram Strait during the last 20,000 years. Quat. Res. 78, 405–416.

Zhuravleva, A., Bauch, H.A., Spielhagen, R.F., 2017. Atlantic water heat transfer through the Arctic Gateway (Fram Strait) during the Last Interglacial. Glob. Planet. Chang. 157, 232–243.